Ion channels that mediate calcium-dependent control of spike patterns are spatially organized across the soma in relation to a cytoskeletal assembly

Giriraj Sahu[†δ1], Dylan Greening[θδ#1], Wilten Nicola[ϒδ] and Ray W. Turner[*θδ#]

Author Footnotes: 1 These authors contributed equally.

[θ]Department Clinical Neuroscience,[ϒ]Department Cell Biology & Anatomy, [δ]Hotchkiss Brain Institute, #Alberta Children's Hospital Research Institute, Cumming School of Medicine, University of Calgary, Calgary, Alberta, Canada T2N 4N1, [†]Molecular Biophysics Unit, Indian Institute of Science, Bangalore-560012, India

Running title: Somatic organization of a CaRyK complex

Figures: 11
Supplemental Figures: 4
Supplemental Tables: 5

Key words: Cav1, KCa3.1, RyR2, spectrin, cytoskeleton, ER-PM junction, hippocampus

*** Corresponding Author:**
Ray W. Turner
Health Res Innovation Ctr 1AA14
3330 Hospital Dr. N.W.
University of Calgary, Calgary, Alberta
Canada T2N 4N1
(403) 220-8452
FAX (403) 210-7446
Correspondence: rwturner@ucalgary.ca

Declaration of Interests:
The authors declare no competing interests.

Abstract (181 words)
Sodium and potassium channels that regulate axonal spike propagation are highly organized at nodes of Ranvier by a spectrin-actin membrane periodic skeleton. STORM-TIRF microscopy was used to define the spatial organization over the soma of a complex of Cav1.3 calcium, RyR2, and IK potassium channels (CaRyK complex) that generate a slow AHP in hippocampal neurons. Nearest neighbor distance and non-negative matrix factorization analyses identified two spatial patterns as linear rows of 3-8 immunolabeled clusters with 155 nm periodicity that extended to branchpoints, or as isolated clusters with 600-800 nm separation. The rows and isolated clusters for each of the CaRyK complex proteins closely overlapped with the patterns for spectrin βII and the actin linking proteins actinin I and II. Together the data reveal a close correspondence between the placement of CaRyK complex proteins and that of a net-like organization of spectrin βII across the soma. The regularity in the pattern of expression of these proteins at ER-PM junctions suggest their role as functional nodes of calcium- and calcium-gated potassium channels to control the pattern of spike output at the soma.

Introduction (493 words)
Intrinsic ionic mechanisms at the level of neuronal somata integrate synaptic inputs to shape spike output. Central to this process are calcium and calcium-gated potassium channels that together generate the after-hyperpolarizations (AHP) that pattern spike output into bursts and pauses. Yet the mechanisms by which calcium and potassium channels are spatially organized to control spike output remains to be determined. In hippocampal neurons a triprotein complex comprised of Cav1.x calcium channels, ryanodine receptor 2 (RyR2), and KCa3.1 (IK) potassium channels (CaRyK complex) formed at ER-PM junctions contributes to generating a slow AHP of several seconds duration (Higham et al., 2019; King et al., 2015; Sahu et al., 2019, 2017; Sahu and Turner, 2021; Tiwari et al., 2022; Turner et al., 2016; Wang et al., 2016). The factors that govern expression of the CaRyK complex are important as the slow AHP controls spike output in normal and disease states, and circuit function with age (Moore and Murphy, 2020; Sahu and Turner, 2021; Tiwari et al., 2019).

It is known that efficient propagation of spikes down an axon depends on the precise localization of sodium and potassium channels at the axon initial segment (AIS) and axon nodes of Ranvier (D'Este et al., 2017; Trimmer, 2015; Zhou et al., 2022). It was recently shown that the axon exhibits a membrane periodic skeleton (MPS) where lengths of spectrin running parallel to the axon support periodic circumferential bands of actin (D'Este et al., 2015; Han et al., 2017; Lorenzo et al., 2023; Unsain et al., 2018; Xu et al., 2013; Zhong et al., 2014; Zhou et al., 2022). Sodium and potassium channels are localized at the AIS and axonal nodes by linking to the spectrin-actin MPS with a semi-periodic "1D" distribution (D'Este et al., 2017; Maverick and Tamkun, 2022; Unsain et al., 2018; Xu et al., 2013; Zhou et al., 2022). By comparison, a "2D" configuration of spectrin was reported over regions of the somatic membrane of cultured neurons (Han et al., 2017). It is not known if spectrin could play a role in coordinating the expression of the CaRyK complex across somatic membrane.

We used stochastic optical reconstruction microscopy (STORM) with total internal reflectance fluorescence (TIRF) illumination to assess the spatial distribution of the CaRyK complex and its relationship to the cytoskeleton at the soma of hippocampal neurons. Calculations of nearest neighbour distance and non-negative matrix factorization revealed two patterns of immunolabel for CaRyK complex proteins across the entire somatic surface. One was a linear series (row) of 3-8 punctate clusters with a periodicity

of ~155 nm that could reach and extend beyond branch points, and the second was isolated clusters positioned at peak distances of ~600-800 nm. Both patterns also proved to be evident in immunolabel for spectrin βII and actinin linking proteins that colocalized with CaRyK complex proteins. Together these data reveal an organized pattern of the CaRyK complex that is distributed across the soma in relation to a 2D spectrin-based cytoskeletal structure.

Results

STORM-TIRF imaging was used to localize CaRyK complex proteins within 150 nm of the coverslip surface of MAP-2 positive cultured neurons. Images were defined with 10-25 nm localization precision of individual fluorophore centroids. As previously discussed (Higham et al., 2019; Sahu et al., 2019) immunolabels were not assumed to reflect individual ion channels, with a group of fluorophore labels defined by STORM referred to only as clusters. Cluster analysis was performed using masks that included the lateral membrane borders and entire surface of somatic membrane, but not dendritic or axonal processes outside of this region. Nearest neighbour distance (NND) and non-negative matrix factorization (NNMF) calculations were applied to typically >500 clusters per label/cell (675 ± 26; n = 279) and up to 43,000 clusters in up to 55 cells per label for statistical analyses.

CaRyK complex proteins exhibit a high degree of organization across somatic membrane

STORM-TIRF imaging of immunolabels for proteins that comprise the CaRyK complex revealed discrete labeling of clusters across the entire somatic membrane (***Figure 1 and 2***). We first focused on cells dual labeled for Cav1.3 and IK immunofluorescence. An extensive distribution of clusters could be resolved at larger fields of view (***Figure 1A***) or in magnified ROIs (***Figure 1B***) as punctate labels detected in isolation or with discrete overlap of the alternate fluorophore. A distinct pattern was apparent for both IK and Cav1.3 as 3-8 closely spaced (rows) of clusters (see also ***Figure 7A***). Rows of clusters could further meet at junction points (***Figure 1B***) from which 1-2 branches of similarly spaced rows of clusters extended at angles of 70-150 degrees (IK, 120 ± 1.59 degrees, n = 101; Cav1.3, 118 ± 2.33 degrees, n = 103) (see also ***Figure 7B***). It was difficult to pinpoint a dominant label for Cav1.3 or IK, as rows of clusters could be detected for either IK or Cav1.3 (***Figure 1B*****,** ROI-3 and 4), with overlap or close association of the other cluster label along a row or at discrete sites that could include the junction point (***Figure 1B*****,** ROI-4 and 6). Clusters of immunolabel could also be detected as being physically isolated from cluster rows with or without close apposition of the alternate label (***Figure 1B,*** ROI-5-7).

NND calculations were carried out using the procedures detailed in the *Materials and Methods.* NND identified two inter-cluster relationships for both IK and Cav1.3 (***Figure 1C and 1D***). For IK clusters one was fit over a short distance of <500 nm with a median value of 177 nm, and a second over a larger range of up to ~2000 nm with a median value of 699 nm (***Figure 1C***). A similar dual distribution of minimal distance was apparent between Cav1.3 clusters up to ~400 nm and ~2000 nm, with median values of 169 nm and 664 nm, respectively (***Figure 1D, Supplemental Table 1***). A plot of the minimal distance between neighboring IK and Cav1.3 clusters instead revealed a single right-skewed histogram over a range of up to ~1000 nm and a median value of 188 nm (***Figure 1E***). These data are important in extending our earlier work (Higham et al., 2019; Sahu et al., 2019) by confirming a nanometer association between Cav1.3 and IK clusters consistent with colocalization and two common patterns in the minimal distance between IK and Cav1.3 immunolabels.

Detecting patterns of protein distribution

The ability to consistently define two patterns of cluster distances between Cav1.3 and IK immunolabels suggests a non-random distribution of CaRyK complex proteins across the somatic membrane. To test this we randomized the centroid positions for each of the CaRyK protein data sets. These tests returned unimodal histograms consistent with spatially random data that were distinct from those of experimental data (***Supplemental Figure 1***).

To more fully assess the spatial patterns of these labels we conducted NNMF analysis to extract the top 6 detectable patterns (features) of immunolabel clusters in each cell for analysis (see Materials and Methods*,* ***Figure 9 and 10***). A key advantage to NNMF is the ability to define features beyond the minimal nearest neighbor for every cluster centroid without the need to identify the specific orientation of Regions of Interest (ROI) (Berry et al., 2007). As a crosscheck of this approach we compared NNMF to the alternate method of autocorrelation applied to predefined ROIs for spectrin βII in the MPS in axons and dendrites (Han et al., 2017; Zhong et al., 2014) and obtained very similar spatial separations between spectrin repeats of ~155 nm (***Figure 11***). It is of interest that these values are somewhat shorter than previous reports of an average value of ~180-190 nm (D'Este et al., 2017; Han et al., 2017; Xu et al., 2013). We consider this to reflect the elasticity inherent to a resting spectrin framework (Brown et al., 2015; Grum et al., 1999; Nans et al., 2011), or potentially the relative length of spectrin isomers incorporated into the developing cytoskeleton at ~DIV 10-15 (Han et al., 2017; Huang et al., 2017; Machnicka et al., 2012; Zhong et al., 2014) (see Discussion).

We therefore used NNMF as an objective, automated process to define meaningful patterns of immunolabel clusters at the soma. To identify relationships between immunolabeled clusters with putative colocalization (i.e. IK and Cav1.3) (Sahu et al., 2019), we restricted NNMF analysis to only the centroids of clusters identified to exhibit overlap in fluorescence between the two labels (***Supplemental Figure 2***).

CaRyK complex proteins exhibit a regular pattern of expression

IK and Cav1.3

NNMF was applied to IK and Cav1.3 clusters to assess the periodicity of rows of clusters as well as isolated clusters. Features extracted by NNMF analysis that reflected a row of clusters were fit by a damped oscillatory model to identify a period for IK clusters of 139 nm (***Figure 1F, Supplemental Table 2***). Features with a repeating pattern between Cav1.3 clusters exhibited a period of 159 nm (***Figure 1G***). When comparing the relationship between colabeled IK-Cav1.3 clusters, NNMF again reported a regularity with a period of 156 nm (***Figure 1H***). To define potential patterns in the distant (isolated) group identified through NND calculations (***Figure 1C and 1D***), we extracted features with peaks separated by distances of 375-1506 nm. This second group of features could be described with a single gamma fit, returning median values for isolated IK-IK clusters of 679 nm and for Cav1.3-Cav1.3 clusters 638 nm *(**Figure 1I and 1J***). By comparison, the relationship between colabeled isolated IK and Cav1.3 clusters was fit with a median of 795 nm (***Figure 1K***).

These tests established a high degree of shared spatial regularity of IK and Cav1.3 labels as rows of tightly spaced clusters ~140-160 nm apart or as isolated clusters separated on average by ~600-800 nm (***Supplemental Table 2***). A colocalization of immunolabels for IK and Cav1.3 could be detected for both rows and isolated cluster patterns of distribution.

RyR2 relationship to Cav1.3 and IK

Previous work established that RyR2s are colocalized with nanometer proximity to Cav1.3 and IK channels as part of a CaRyK complex at ER-PM junctions (Sahu et al., 2019; Sahu and Turner, 2021; Vierra

et al., 2019; Vierra and Trimmer, 2022). Immunolabeling for RyR2 confirmed an extensive distribution across the soma and a colocalization with Cav1.3 and IK labels that gave rise to many similarities in the spatial pattern for RyR2 (***Figure 2A-D)***. RyR2 clusters could thus be visually distinguished as rows of clusters that converged at branch points from which other rows of clusters labeled for RyR2 and/or the counter-labeled protein could extend (mean angle, 116 ± 1.51 degrees, n = 100) (***Figure 2B, 2D, 7B***). RyR2 clusters could also be identified in isolation with or without overlap of an ion channel fluorophore emission suggestive of colocalization (***Figure 2B and 2D***). The latter results are important in emphasizing that RyR2 labeling was not obligatory with Cav1.3 or IK labeling but could exhibit a high degree of co-organization in expression within the 150 nm distance from the surface of the coverslip defined by TIRF imaging.

NND analysis confirmed a separation of RyR2 cluster distances into one group with a median for distance to nearest neighbor of 185 nm and a more dispersed group with a median of 755 nm (***Figure 2E***). NND calculations between RyR2 clusters and those for Cav1.3 or IK channels returned right-skewed interval histograms with a median of 238 nm for RyR2-Cav1.3 and 238 nm for RyR2-IK (***Figure 2F and 2G***). Applying NNMF analysis to these two populations revealed a high degree of spatial organization of RyR2-RyR2 clusters. Specifically, repeating clusters for RyR2-RyR2 were fit by a damped oscillatory model with a period of 158 nm (***Figure 2H***). NNMF analysis also revealed a repeating pattern of clusters for RyR2-Cav1.3 with a period of 158 nm and for RyR2-IK a period of 123 nm (***Figure 2I and 2J***). The spatial relationship between isolated clusters for RyR2 was fit over a larger range of distances, with median values between clusters of RyR2-RyR2 of 689 nm, RyR2-Cav1.3 of 819 nm, and RyR2-IK of 810 nm (***Figure 2K-M***).

Altogether these analyses confirmed a close spatial relationship between RyR2 and CaRyK complex ion channels that co-distributed as either rows of clusters or isolated clusters. These values are also important in highlighting the extent of co-distribution of a RyR2 calcium release channel in the ER to Cav1.3 and IK channels that together signify the position of one class of ER-PM junctions.

The spatial pattern of CaRyK complex proteins reflects coassociation with the spectrin cytoskeleton

The coordinated patterns of expression of CaRyK complex proteins across the somatic membrane imply the presence of an underlying mechanism for organization. It is known that the spatial distribution of sodium and potassium channels in axons is determined by a spectrin-actin-based MPS (D'Este et al., 2016, 2015; Han et al., 2017; He et al., 2016; Xu et al., 2013; Zhong et al., 2014; Zhou et al., 2022). While this "1D" MPS structure can also be found in portions of dendrites (D'Este et al., 2015; Han et al., 2017; Xu et al., 2013; Zhong et al., 2014), evidence points to a "2D" structure formed by spectrin in the somatic region (Han et al., 2017). Several isoforms of spectrin are expressed in neurons (Lorenzo et al., 2023; Machnicka et al., 2012; Unsain et al., 2018) with the extent of a 1D structure in dendrites related to the level of spectrin βII (Han et al., 2017; Zhong et al., 2014). We thus used labeling for the C-terminus of spectrin βII to test for any spatial relationship with respect to the organization of CaRyK complex proteins.

Spectrin βII and CaRyK complex proteins

We found that spectrin βII immunolabel could be visualized over the entire region of hippocampal neuron somata (***Figure 3***). As found for CaRyK complex proteins, punctate clusters of spectrin βII were detected aligned in rows that would reach branch points where 1-2 rows of clusters could extend at angles

with a mean of 118 ± 1.63 (n = 104), or as isolated clusters (***Figure 3A-D***). In dual labeled cells spectrin βII and Cav1.3 exhibited close alignment that resulted in overlap or close apposition of fluorophore emissions (***Figure 3C and 3D***). In some cases the labels were complementary such that labeling of rows of either spectrin βII or Cav1.3 clusters could effectively bridge a row of labels towards an apparent branch point (***Figure 3D***).

Quantitative analyses revealed many similarities in the patterns of distribution for spectrin βII and Cav1.3 labeling. NND calculations between spectrin βII clusters revealed two populations with a short inter-cluster distance of less than ~400 nm with a median of 176 nm, and a second broader distribution up to ~2000 nm with a median of 733 nm (***Figure 3E***). The histogram for NND between spectrin βII and Cav1.3 clusters was right-skewed with a median of 288 nm, indicating a preferred close spatial relationship (***Figure 3F***). NNMF analysis of spectrin βII - spectrin βII clusters at the soma identified a repeating pattern with a period of 159 nm (***Figure 3G***), similar to that determined for spectrin βII clusters in neural processes (see ***Figure 11***). NNMF calculations for cells co-labeled for spectrin βII and Cav1.3 also identified a regularity in overlapping labels with a period of 134 nm *(**Figure 3H***). NNMF applied to isolated clusters identified distances between spectrin βII clusters of 746 nm and between spectrin βII and Cav1.3 clusters of 917 nm (***Figure 3J***).

Immunolabeling for spectrin βII and either IK or RyR2 revealed similar relationships in organization and pattern as that for Cav1.3. Immunolabeling for spectrin was detected with close association to IK or RyR2 clusters either as rows or as isolated clusters (***Figure 4A-D***). IK and RyR2 immunolabels could also be distributed as a segment of rows of clusters that alternated with a row of spectrin βII clusters (***Figure 4B and 4D***). In dual-labeled cells, NND calculations revealed two populations for each of spectrin βII with IK and RyR2 clusters, with an early peak and another with a broader distribution (***Supplemental Figure 3***). By comparison, NND analysis returned right-skewed histograms for IK-spectrin βII with a median value of 238 nm and RyR2-spectrin βII 288 nm (***Figure 4E and 4F***). NNMF analysis of colabeled clusters identified a regular distribution of rows of clusters for IK-spectrin βII (period of 121 nm) and for RyR2-spectrin βII clusters (period of 160 nm) (***Figure 4G and 4H***). The pattern for co-labeled isolated clusters identified a distribution for IK-spectrin βII with a median of 743 nm and for RyR2-spectrin βII 889 nm (***Figure 4I and 4J***).

These data are important in revealing that two patterns of spatial organization found for each of the three subunits of the CaRyK complex essentially match that of spectrin βII as an indicator of the underlying cytoskeleton.

Actinin I and II linking proteins

Ion channels in the membrane connect to the actin-spectrin cytoskeletal matrix through intermediate linking proteins. Key to this is a family of spectrin proteins that form a meshwork to interlink membrane ion channels with the cytoskeleton (Liem, 2016). Actinins are closely related to spectrin and form extended rod-shaped molecules that act to cross-link actin filaments that in turn connect to spectrin (Liem, 2016). Previous work has shown roles for actinin I and II in controlling the organization of ion channels specifically relevant to subunits in the CaRyK complex (Hall et al., 2013; Hiess et al., 2015; Lu et al., 2009, 2007; Sadeghi et al., 2002; Turner et al., 2020; Zuccotti et al., 2011).

Actinin proteins and spectrin βII: To investigate the spatial organization of actinin proteins we dual labeled hippocampal neurons for spectrin βII and either actinin I or actinin II. These tests revealed a high degree of co-distribution of spectrin βII and actinin proteins either as overlapping or adjacent immunolabels (***Figure 5***). Both actinin I and II were expressed as rows of clusters that could reach branchpoints

(***Figure 5B and 5D***) at angles for actinin I of 115 ± 2.7 (n = 52) degrees and actinin II of 118 ± 1.8 (n = 120) degrees. Actinin immunolabels could further overlap or alternate with rows or isolated clusters of spectrin βII (***Figure 5B and 5D***). NND calculations revealed two populations of actinin I or actinin II with one at short distances (median values: actinin I, 179 nm; actinin II, 161 nm), and a second over a longer and broader distribution (median values: actinin I, 516 nm; actinin II, 498 nm) (***Supplemental Figure 4A and 4B***). NNMF analysis identified a periodic distribution of clusters for actinin I of 164 nm and actinin II of 159 nm, with isolated clusters separated by a median value of ~685 nm (***Supplemental Figure 4C-F***).

In dual labeled cells histograms of the distance between neighboring actinin and spectrin βII proteins were right-skewed with a median value for actinin I-spectrin βII of 163 nm and for actinin II-spectrin βII of 188 nm (***Figure 5E and 5F***). NNMF analysis confirmed a repeating organization for actinin I-spectrin βII with a period of 141 nm and for actinin II-spectrin βII of 177 nm (***Figure 5G and 5H***). A spatial relationship was also apparent for isolated clusters with interpeak distances for actinin I-spectrin βII of 960 nm and actinin II-spectrin βII of 939 nm (***Figure 5I and 5J***). These data establish that key actin-linking proteins distribute with a similar pattern of organization as that of spectrin βII.

Actinin proteins and the CaRyK complex: We then examined the spatial relationship between CaRyK complex proteins and actinin I and actinin II. Dual labeled images indicated a very tight association between clusters for actinins and each of Cav1.3, IK, or RyR2 (***Figure 6A-F***). Immunolabeled clusters were distributed in tightly spaced rows that exhibited strong overlap or alternation in segments of cluster labels between actinin I and Cav1.3, actinin II and IK, and actinin II and RyR2 (***Figure 6B, 6D, and 6F***). Indeed, the extent of colabeling of actinin II cluster rows with IK or RyR2 provided some of the clearest labeling of a pattern consistent with an underlying spectrin-based architecture (***Figure 6C-F***) (Hall et al., 2013; Lu et al., 2009). NND analysis restricted to clusters of actinin and CaRyK complex proteins exhibiting overlap presented interval histograms that were strongly right skewed, with median values between different pairs of clusters ranging from 138-213 nm (***Figure 6G-I***). NNMF analysis also confirmed regularity between colabeled actinin and CaRyK complex protein clusters with periods of 147-160 nm (***Figure 6J-L, Supplemental Figure 4-F***). NNMF analysis of isolated clusters of overlapping actinin and CaRyK complex proteins again returned median values over longer distances of 730-790 nm (***Figure 6M-O***).

Correspondence between the spatial organization of CaRyK complex and cytoskeletal proteins

One of the most striking parallels in the spatial organization of cytoskeletal and CaRyK complex proteins was in colabeling rows of clusters that reached or extended beyond branchpoints. To further compare these parameters, we examined rows of clusters at high resolution in up to 5 randomly selected ROIs of 600 X 600 pixels / cell drawn from 13-55 cells per label. Up to 388 rows for CaRyK complex proteins and spectrin βII were defined across a selection of up to 275 ROIs and 55 cells (***Figure 7A***). Comparing the number of clusters per row returned very similar histogram distributions for each of the CaRyK complex proteins. Approximately 50-60% of all clusters were contained within rows of 3 clusters, with a decrease in number to ~20-25% of clusters in rows of 4, and to only a few percent in rows containing up to 8 clusters (***Figure 7A***). By comparison, ~40% of spectrin βII clusters were contained in rows of 3 clusters, with a similar decrease in number from 4-8 clusters per row (***Figure 7A***).

We further measured the angles formed at branch points of rows for CaRyK complex proteins and spectrin βII. Measurements were drawn for rows of least 3 consecutive clusters that reached a point where a second row of clusters extended with a shift in orientation. Approximately 100 branch points

were measured by two viewers for each label across 22-52 ROIs randomly selected from 13-18 cells. In each case, branch points were formed at angles that ranged between 60-180 degrees centered on a mean value of 118 ± 1.63 degrees (n = 104) (***Figure 7B***). No statistical difference was found between any of the distributions of angles for branch points of rows of CaRyK proteins, spectrin βII, or actinin proteins (***Supplemental Table 3***).

Additional comparisons were made for fits obtained by the model for cluster rows and fits for isolated clusters (***Figure 7C-J***). The close spatial relationship between CaRyK complex proteins was emphasized in the model fits for rows of Cav1.3-Cav1.3 and RyR2-RyR2 that were entirely superimposed with periods of ~158 nm (***Figure 7C***). The fit for the period of IK-IK cluster rows overlapped these distributions, although the period was ~19 nm shorter (***Figure 7C***). When comparing the spatial pattern for pairs of CaRyK proteins that exhibited overlap in emissions, the model fits for Cav1.3-IK and Cav1.3-RyR2 showed closely aligned peaks with periods of ~157 nm (***Figure 7D***). By comparison, the model fit for the period of IK-RyR2 clusters presented with a shorter relative period in which crests peaked ~34 nm shorter than for Cav1.3-IK and Cav1.3-RyR2 labels (***Figure 7D***). The spatial regularity revealed by NNMF for CaRyK complex proteins in relation to spectrin βII also showed a close correspondence, particularly for spectrin βII-Cav1.3 (134 nm) and spectrin βII-IK (121 nm) (***Figure 7E***). The period of cluster rows for spectrin βII-RyR2 (160 nm) conformed somewhat less to the fits for Cav1.3 and IK, with a period ~30-40 nm longer (***Figure 7E***). By comparison, the model fits for the relationship between rows of clusters labeled for actinin I or actinin II with respect to spectrin βII almost perfectly superimposed (~160 nm) (***Figure 7F***), emphasizing the close spatial relationship between these proteins.

Comparison of the fits for the spatial distribution of isolated clusters of CaRyK complex proteins were generally very consistent in revealing a peak inter-cluster distance of ~650 nm (***Figure 7G***). Fits of the distributions between isolated clusters of overlapping CaRyK complex proteins reported the same relative median of ~800 nm and a particularly narrow distribution for Cav1.3-IK consistent with a tight functional coupling between these proteins (***Figure 7H***). Similarly, fits for the distance between isolated clusters of spectrin βII and both Cav1.3 and RyR2 superimposed with median values of ~900 nm (***Figure 7I***). Once again the fit for isolated IK-spectrin βII clusters differed somewhat in exhibiting a shorter fit with a median of 743 nm (i.e. ~160 nm difference from spectrin βII-Cav1.3) (***Figure 7I***). The fit for spectrin βII isolated clusters exhibited a median of ~700 nm that overlapped those for actinin I and actinin II (***Figure 7J***).

It is interesting that the periods for IK-IK rows (***Figure 7C and 7D***) or median distance of isolated IK clusters (***Figure 7I***) were somewhat shorter than other proteins. The exact reasons for these differences are unknown, but could be accounted for if IK channels also associate with calcium sources other than the CaRyK complex, such as found for Cav1.2-IK coupling identified in hippocampal cells or a Cav3.2-IK coupling in cerebellar Purkinje cells (Engbers et al., 2012; Sahu et al., 2019). Both RyR2 and RyR3 also functionally couple to potassium channels underlying the sAHP (Sahu and Turner, 2021; Tedoldi et al., 2020), all of which could affect the relative spacing of IK clusters.

Discussion

A highly ordered arrangement of sodium and potassium channels at axonal nodes of Ranvier is enabled by a spectrin-actin MPS that provides control over the expression of ion channels to ensure precision of spike propagation down an axon. However, the pattern and frequency of spikes are more directly controlled by ion channels at the soma that use calcium conductance or internal changes in calcium concentration to modify their level of activation. Specialized ER-PM junctions where the ER reaches to within

15 nm of the somatic plasma membrane can coordinate activity of ion channels and internal calcium release sites to control cell excitability (Dixon and Trimmer, 2023; Fox et al., 2015). One representative assembly at ER-PM junctions is the CaRyK complex studied here that contributes to generating a slow AHP in hippocampal neurons (Higham et al., 2019; King et al., 2015; Sahu et al., 2019; Sahu and Turner, 2021; Turner et al., 2016; Wang et al., 2016). The current study on the spatial organization of the CaRyK complex across the soma reveals that proteins of this complex are not randomly distributed. Rather, the CaRyK complex exhibits a coordinated spatial distribution across the somatic surface consistent with a pattern defined by a spectrin-based cytoskeletal matrix.

Patterns of organization of the CaRyK complex

Both NND and NNMF analyses revealed patterns in the localization of CaRyK complex proteins in the form of rows of clusters with a definable periodicity or as isolated clusters at a longer but predictable distance from its nearest neighbor. Importantly, the definition of these patterns using NNMF was obtained for labels that exhibited overlap in fluorescent emissions consistent with colocalization. The two patterns defined here are thus relevant to protein partners known to interact with nanometer proximities in a CaRyK complex (Sahu et al., 2019). Immunolabeled rows were composed of ~3-8 clusters spaced ~155 nm apart for each of the CaRyK complex proteins. The rows of clusters could further reach branchpoints from which 1-2 additional rows of clusters extended at internal angles of 60-150 degrees (mean of 118 degrees). When viewed with the advantage of dual labeling this process could effectively close a loop in branching structure (***Figure 2B, 2D, 3B, 3D, 5A, 5C, and 6C-F***). These results imply a placement of CaRyK complex clusters according to a common structural system with a branching architecture. Indeed, the distribution of the complex proved to align with that of the spectrin cytoskeleton that presented with a branching pattern across the soma. The relationship between CaRyK complex proteins and spectrin was further indicated by similar patterns and colocalization of actinin I and II that link to actin as part of the cytoskeleton.

A second prominent pattern for CaRyK complex proteins was in isolated clusters that often overlapped in emissions with protein partners at a peak distance of ~600-800 nm. Even labeling for spectrin βII revealed isolated clusters colocalized with CaRyK complex proteins. The reasons for this physical separation of isolated clusters of CaRyK proteins are not yet known, but were routinely identified with a repeatable measure of regularity in relation to the spectrin labeled structure. It needs to be considered that non-conducting Kv2.1/2.2 potassium channels have been shown to control assembly of calcium channels and ryanodine receptors at ER-PM junctions (Antonucci et al., 2001; Dixon and Trimmer, 2023; Fox et al., 2015; Johnson et al., 2019; Lim et al., 2000; Mandikian et al., 2014; Vierra et al., 2019). At this time we do not know the extent to which Kv2.x channels are responsible for organizing the set of patterns observed here for subunits of the CaRyK complex.

Spectrin-based cytoskeletal matrices

The MPS of axons, the AIS, and some dendrites reflect a "1D" pattern consisting of longitudinally oriented spectrin repeats and circumferential bands of actin at regularly spaced intervals (D'Este et al., 2015; Han et al., 2017; Lorenzo et al., 2023; Lukinavičius et al., 2014; Rentsch et al., 2024; Xu et al., 2013; Zhong et al., 2014; Zhou et al., 2022). The somatic surface of neurons has instead been reported to exhibit a 2D structure of spectrin labeling that undergoes an increase in complexity over time to reach ~45% of cell surface area by DIV 28 (Han et al., 2017). The current work also suggests a 2D pattern of

spectrin labeling demarcated by rows of clusters and associated branch points. Our measures of the distance between spectrin repeats at the soma using an antibody against the C terminus of spectrin βII was fit by an oscillatory model as 159 nm ($R^2 = 0.92$) (***Figure 3G***). This compares to average values of the distance between spectrin repeats in the MPS of unmyelinated axons of 180-190 nm (mean of 182 ± 16 nm, range of 150-220 nm) (Xu et al., 2013) and for myelinated axons a mean of 180 ± 35 nm (range of 80-240 nm) (D'Este et al., 2015). The lower value we obtained would be consistent with the known elasticity of spectrin when in a resting state (Grum et al., 1999; Lux, 2016; Nans et al., 2011; Zhou et al., 2022). We note that the matrix-like branching pattern of labels tested here bears a striking resemblance to the polygonal structure naturally adopted by spectrin in structures like that previously defined in erythrocyte membranes (Lorenzo et al., 2023; Lux, 2016; Nans et al., 2011).

ER-PM junctions as ion channel nodes

The CaRyK complex studied here is representative of proteins that are colocalized at specialized ER-PM junctions. ER-PM junctions have previously been shown to coordinate functional outcomes that include endo- and exocytosis, calcium rebalancing, membrane protein delivery, lipid transfer, and excitation-transcription coupling (Antonucci et al., 2001; Deutsch et al., 2012; Fu et al., 2017; Leung et al., 2003; Vierra et al., 2021; Vierra and Trimmer, 2022). ER-PM junctions can also coordinate the expression of calcium channels at the plasma membrane and RyRs in the ER (Dixon and Trimmer, 2023; Fox et al., 2015; Johnson et al., 2019; Sahu et al., 2019; Vierra et al., 2019). The combination of Cav1.3-RyR2-IK proteins studied here as component elements of ER-PM junctions is relevant specifically to generation of a slow AHP (Sahu et al., 2019; Sahu and Turner, 2021). Spikes near the soma can thus activate an intrinsic mechanism at ER-PM junctions to regulate firing rate by activating calcium increases to produce a slow AHP. The current work highlights how CaRyK complex proteins are organized in a 2D pattern correlated to a spectrin-based architecture. The available data would then support a new role for ER-PM junctions (Dixon and Trimmer, 2023) as spatially organized ion channel nodes that colocalize calcium- and calcium-gated potassium channels at the soma to regulate the frequency and pattern of spike output.

Limitations of the current study

We note that the extent to which we could define the full structure of a spectrin-based cytoskeleton was limited by several factors. For one, neurons are known to express tetramers of **α** and different β spectrin subunits (Gao et al., 2011; Lorenzo et al., 2023; Unsain et al., 2018; Zhou et al., 2022) while our labeling was restricted to the spectrin βII C terminus. We further restricted NNMF analysis on dual labeled protein pairs to those exhibiting overlapping fluorescent emissions, reducing the total number of clusters that might align in a given sequence. Our work was also conducted on cultured neurons at ~DIV 10-15 that are mid-stage in development. The spectrin structure visualized here could then reflect an incomplete state of assembly or even transient incorporation of spectrin isoforms with different structural lengths (Lorenzo et al., 2023). For these reasons the full extent of a spectrin-based polygonal structure was likely underestimated. Our current localization precision for STORM reached values of ~10-25 nm. Further improvements in super resolution microscopy can be expected to improve our visualization of the spectrin network and its regulation of somatic ion channel expression patterns.

Materials and Methods

A table of all materials and supplies with catalog numbers, software, and site of data repository is provided in ***Supplemental Table 5.***

Animals

Timed pregnant Sprague Dawley rats were obtained (Charles River) and maintained for at least 7 days after shipping according to the guidelines of the Canadian Council of Animal Care and experimental protocols approved by the University of Calgary Animal Care Committee.

Dissociated hippocampal cell cultures

P0-P1 male or female rat pups were used to prepare low-density dissociated cultures of rat hippocampal neurons (Sahu et al., 2019, 2017). P0-P1 rat pups were anesthetized on ice for 3-5 min and hippocampi dissected and dissociated by papain treatment followed by titration with progressively smaller bore glass pipettes. After each titration step the supernatant containing the cells was passed through a 70 µm separation filter (Corning, Cat. 07201431) into a 50 ml tube. Cells were centrifuged at 300 x g for 10 min and the supernatant completely aspirated. In most cases microglial cells were removed using a mini MACS separator based on an anti-rat CD11b/c antibody conjugated to magnetic microbeads according to manufacturer instructions (Miltenyi Biotec, CA) (Marek et al., 2008). After collecting unlabeled neurons from the column in MACS BSA buffer, basal neural medium (BME) supplemented with 1 mM Na-pyruvate, 2 mM L-glutamine, 10 mM HEPES, 1% B-27 supplement, 5% FBS, 0.6% glucose, and 1% penicillin-streptomycin was added to increase the volume for correct plating density. The cell suspension was then plated on laminin and poly-l-lysine-coated glass coverslips in 12 well culture dishes at 3500–5300 cells/cm^2. Cells were allowed to grow on 18 mm No 1.5 coverslips (Electron Microscopy Sciences, PA) at 37 ºC for three days in BME, followed by complete exchange with BME lacking FBS. Culture medium was refreshed with BME lacking FBS every three days. Cultured hippocampal neurons at 10-15 days *in vitro* (DIV 10-15) were used to obtain images of isolated neurons to further reduce the risk of glial membrane envelopment that could interfere with imaging neuronal proteins adjacent to the coverslip surface.

Immunocytochemistry

At 10-15 days *in vitro* (DIV) coverslips with cells were washed with phosphate-buffered saline (PBS) and fixed in 4% paraformaldehyde (PARA) (Electron Microscopy Sciences, ON) in PBS for 10-15 min. After 3 washes in PBS cells were incubated with a blocking medium consisting of (5% (w/v) bovine serum albumin (Vector Laboratories) and 0.2% (v/v) Triton X-100 (Sigma Aldrich) in PBS for 45 min at room temperature (RT) (~25°C) for all subsequent treatments. Cells were incubated with primary antibodies (Key Resource Table) in blocking medium for 45 min at RT. After five 10 min washes in blocking medium cells were treated with the secondary antibodies for 45 min at RT. After three rounds of 10 min washes in blocking solution cells were washed once in PBS and post-fixed with 4% PARA and 0.1% glutaraldehyde in PBS for 10 min followed by three 10 min washes in PBS. TetraSpek™ beads (1:2000, 100 nm diameter, T7279, Thermofisher) were added to coverslips overnight at 4ºC in PBS followed by three 5 min washes in PBS to remove loose beads.

Direct Stochastic Optical Reconstruction Microscopy (dSTORM)

STORM imaging was used together with TIRF illumination to localize CaRyK complex proteins within 150 nm of the coverslip surface of MAP-2 positive cultured neurons. Imaging cocktail was prepared

fresh from 1X PBS, 10% (w/v) glucose, 10 mM β-mercaptoethanol in an oxygen-scavenging GLOX solution containing 0.5 mg/ml glucose oxidase and 40 µg/ml catalase (Sigma-Aldrich). 10X GLOX solution was prepared as a stock and stored in aliquots at −20°C. On the day of imaging an aliquot of GLOX solution was used to prepare the dSTORM imaging buffer. Imaging cocktail was placed into a concavity slide, covered with the immunolabeled 18 mm coverslip and sealed with VALAP (equal parts vaseline, lanolin and paraffin). Images were obtained using a Quorum Diskovery Flex microscope equipped for TIRF illumination (150 nm depth) using a HC Plan Apo 63X/NA 1.47 oil immersion objective and Andor iXon Ultra 897 EMCCD camera. Fluorophores were first photo switched into a temporary dark state using strong intensity laser illumination (laser power: 561 nm, 55 mW @ 100%; 647 nm, 53 mW @ 100%). Subsets of active blinking fluorophores were then imaged at a lower laser intensity (70-95% excitation) using a 33 Hz frame rate. The 405 nm laser line was adjusted to obtain a balanced reactivation of Alexa Fluor-647 or Cy-3 dyes during image acquisition of 5000-8000 frames per sample.

Image reconstruction was carried out as previously described (Sahu et al., 2019) using a ThunderSTORM plugin (Fiji, ImageJ). A calibration factor of 150.5 nm / pixel was obtained under our imaging conditions after rigorous calibration using a slide mounted Supracon nanoscale standard linewidth/pitch target (Part number Kali2020_2_F5; Supracon, Germany) (Live Cell Imaging Facility, University of Calgary). The acquired images were filtered using the wavelet filter function of ThunderSTORM with default values (beta spline order of 3 and a scale of 2), for determining signal-to-noise threshold for the datasets. The camera parameters used were pixel size: 150.5 nm; photoelectrons per A/D count: 8.98; base level A/D count: 200; EM gain: 300. Afterward, the point spread function of the imaged fluorophore localizations were detected with the standard gaussian filter method and fitted with a weighted least square fitting using the subpixel localization fitting procedure of ThunderSTORM. Only the localizations falling under a standard deviation of the fitting distance, representing sigma >50 and <500 were taken into further analysis. Any mechanical drift over the timeframe required for imaging over 15-20 min (0 to <500 nm) was drift corrected using the cross correlation function of ThunderSTORM, with any cases approaching 700 nm excluded from analysis. Correct image reconstruction and alignment for dual labeled images were assured using the X-Y coordinates of 3-6 100 nm fiducial beads (T7279, Thermofisher) as reference points to align signals with an affine/linear registration function using Localization Microscopy Analyzer (LAMA) (Malkusch and Heilemann, 2016). X and Y positional coordinates and intensity information of point localizations were analyzed using the morphological cluster analysis pipeline of LAMA software to identify the coordinates of protein clusters with a minimum cluster radius of 25 nm.

Image Analysis

Extensive work on the pattern of actin and spectrin labeling in axons and dendrites has defined a structural entity referred to as a Membrane Periodic Structure (MPS) (D'Este et al., 2015; Han et al., 2017; Lorenzo et al., 2023; Unsain et al., 2018; Xu et al., 2013; Zhong et al., 2014; Zhou et al., 2022). Obtaining a measure of the periodicity of proteins along the MPS was obtained using autocorrelation on ROIs that defined the linear projection of given axons or dendrites. The issue is more complicated in somatic regions where even closely spaced immunolabel clusters could project in any x-y coordinate. For this reason both NND and NNMF were used to systematically search through pixels in an ROI that included the lateral borders and entire cytoplasmic region of the soma defined by MAP2-GFP labeling.

Analysis of spatial relationships was carried out on either single immunolabels or on centroids reflecting an overlap of fluorophore emissions by calculating the square-root of pixel intensity product (***Supple-***

mental Fig. 1). While the extraction of centroids with overlapping pixels served to eliminate single labeled clusters, we note that it also had the effect of underestimating the total number of co-associated clusters that appeared to be in immediate apposition, if only through a function of parallax of vertically aligned proteins. For example, for cells dual labeled for spectrin βII and Cav1.3, the total number of spectrin βII centroids was 6,741. The process of extracting spectrin βII clusters that overlapped with Cav1.3 clusters reduced the detected spectrin βII centroids by 53% to a total of 3,191. Despite these reductions in centroids detected, NNMF analysis typically applied to 8-13 dual labeled cells with 900-5,100 centroids that generated 9-22 features for clusters associated in rows and 14-34 features for isolated clusters. Analysis of the percentage overlap of colabelled CaRyK protein clusters as determined by the portion of pixels with intensity higher than a threshold of 0.2 in both channels is shown in ***Supplemental Table 4***.

Nearest Neighbour Distance (NND)

Intensity information and close proximity of individual fluorophores of the ThunderSTORM/LAMA reconstructions were used to create a mask and identify immunolabeled clusters using the standard morphological cluster analysis (MCA) module of LAMA (Higham et al., 2019; Malkusch and Heilemann, 2016; Sahu et al., 2019). Cluster centroid information obtained from MCA analysis was used to determine nearest neighbour Euclidean distances in MATLAB (Higham et al., 2019; Sahu et al., 2019). Distributions were computed for each immunolabel cluster set (eg. Cav1.3-Cav1.3, Cav1.3-RyR2) and fit with either a single gamma distribution or a gamma mixture model using the MATLAB function *lsqnonlin* to define central tendency of the sub-populations in the distributions (Vegas-Sánchez-Ferrero et al., 2014). Mixing portions are the integral of each gamma distribution in comparison to the integral of the gamma-mixture model. To assess the spatial randomness of clusters, the NND distributions were further compared to that of the same number of centroids with randomized positions and histograms assessed with the Kosmolgov-Smirnov test in MATLAB (***Supplemental Fig. 1***).

Non-negative matrix factorization (NNMF)

NNMF is a computational algebraic tool for reducing dimensionality in data (Berry et al., 2007). As a form of singular value decomposition, NNMF generates two matrices reflecting a collection of 'features' and weights', of which the product approximates the input data. A strength of NNMF is its capacity to define patterns within a dataset when data has been standardized. Ultimately NNMF provides a means to compress hundreds of standardized images and reduce them into a handful of 'feature' images (for reviews see (Berry et al., 2007; Wang and Zhang, 2013)).

A brief summary of the process for NNMF analysis used here is presented in ***Figure 8-11*** for the case of spectrin βIIC imaged in neural processes external to the soma, with parameters used for extracting features from somatic labels applied to these images. First, STORM-TIRF images confirmed that the resolution of our system was sufficient to identify the repeating domains of spectrin βII in both MAP2 negative (presumed axons) and MAP2 positive (presumed dendrites) of cultured neurons consistent with an MPS structure (***Figure 11***). Images were prepared for NNMF analysis using a MATLAB script which normalized image intensities and identified centroids through image segmentation using the *regionprops* function. To standardize pattern detection for clusters initially oriented in any x-y direction, ROIs centered around every centroid position were stored as 2D 600-X-600 pixel (4.5 X 4.5 µm) images and rotated so the nearest centroid was oriented to the left (***Figure 8A-C***). The MATLAB function *nnmf,* from the 'machine learning toolbox', with the default alternating least squares algorithm, and random initialization matrices was used.

Images at the soma (***Figure 1-3***) identified two broad classes of cluster organization identified by NND analyses: one with closely repeating peaks and another with few peaks and greater spatial separation. Long segments of repeating spectrin clusters were particularly evident in neural processes even though isolated clusters were also detected (***Figure 8D-G***). NND analysis in neural processes confirmed a high proportion of clusters separated with a periodicity of 144 nm, as well as a smaller population of longer inter cluster distances (***Figure 8D***). Since these patterns at the soma were typically contained within a distance of 1200 nm on NND distributions and ~150 subpixels on 1D cluster intensity profiles of aligned images, feature categorization of spectrin βII by NNMF in neural processes was restricted to a window of -150 to 100 subpixels (-1128 nm to 752 nm).

NNMF was employed to derive 6 features from the collection of 118 to >2000 (668 ± 25) centroid images stored from each image channel per cell (Berry et al., 2007). Extending the number of features beyond 6 resulted in instances where the centering centroid required as a reference point from which inter-cluster distances were measured, was diminished or absent in features (***Figure 9A***). Extracting 6 feature sets from the data reduced this deviation from the true images while still maximizing the number of features to process and the quality of the approximations (***Figure 9B and 9C***). Examples of 6 features extracted from spectrin βIIC labeled neural processes external to the soma of a single cell are shown in ***Figure 9D***. After smoothing with *spaps*, peaks in the 1D feature data were detected using the *findpeaks* function with a minimum distance, prominence, and height threshold of 12, 0.1% of max, and 5% of max, respectively. 1D features were then classified as regularly spaced clusters (rows) (***Figure 8F***) when 4 or more peaks were found in the detection window, or isolated clusters when 2 or 3 peaks were located (***Figure 8G***). Features with less than 2 peaks were discarded.

Comparison of NNMF to correlation

To fully validate the use of NNMF, we tested its ability to quantify the MPS pattern of spectrin βIIC labeling in neuronal processes compared to conventional autocorrelation (***Figure 10***). STORM-TIRF images of spectrin in MAP2-positive or MAP2-negative processes outside of the soma provided well defined rows of closely spaced clusters for spectrin βII (***Figure 10A and 10B***). Autocorrelation was applied to 28 of each of these classes of spectrin βII labeled clusters outside of the soma to derive a period of 152 ± 2.38 nm (n = 7) for MAP2 negative processes (***Figure 10C***). Application of NNMF to MAP2 negative processes calculated a period of 148 nm (R^2 = 0.9) (***Figure 10D***). While the period derived by autocorrelation and NNMF are statistically different (p = 0.010, t-stat = 2.6393) the mean values differed by less than 3%. In comparing the results for MAP2 positive datasets, autocorrelation returned a period of 156 ± 4.34 nm and NNMF a period of 157 nm (R^2 = 0.84), results that were not significantly different (p = 0.752, t-stat = 0.3234) (***Figure 10C and 10D***).

Fitting of row periods and isolated cluster distances

On the basis of these forms of analyses we applied NNMF to extract features to define the periods of regularly spaced clusters by fitting inter-peak distances with a damped oscillatory model (**Eq. 1**) using *lsqnonlin* in MATLAB (***Figure 11A and 11B***). Fitting this model along the entire data range (***Figure 10D***) yielded interpretable results but was optimized to the range of 112-526 nm. The lower limit of this was chosen just within a limit set by the peak detector (90 nm). The higher limit was to ensure the models were fit to the highest signal-to-noise region of the data, and match the most common row length (3 clusters) observed in the soma (***Figure 7A***).

Eq. 1 $f(x) = Ae^{(-ax)} cos(\frac{2\pi}{T}(x + \Phi)) + ye^{(-vx)}$

Equation 1 variables: A = amplitude; α = amplitude decay; T = period; Φ = horizontal phase shift; y = baseline; v = baseline decay

Optimal fitting was performed on raw and smoothed data (***Figure 11A and 11B***) using preset and user specified initial values for the least squares solver. This raw and smooth data was amplitude normalized prior to initial value selection to make user values more predictable (***Figure 11B***), but rescaled to the original data after fitting. Four iterative fits were performed using each initial value set with increasing freedom in the parameters (***Figure 11B***). The parameters that generated the smallest SSQ in the third or fourth fit were used to define the oscillatory model reported.

Isolated features were examined in a window of -376 to -1506 nm (***Figure 11F***) from the centering cluster to ensure analysis avoided interpretation of very distant clusters and that gaussian fitting was not disrupted by the tails of the centering centroid. Single gaussian fits were applied to data in the examination window using the function *fit*. These gaussian models were used as proxies of the peak data as isolated point-spread-functions are expected to have a gaussian distribution. The standard deviation and mean of these fitted gaussians were plotted on two axes to identify the number of populations in each data set (***Figure 11G***). Outliers in either standard deviation or mean of the gaussian fit were identified and culled using the function *rmoutliers* in MATLAB (***Figure 11G***). Remaining gaussian distributions with means outside of the initial examination window (-376 to -1506 nm) or an excessive standard deviation (SD >= 400) were removed. Finally gaussians with a poor goodness of fit ($R^2 \leq 0.9$) were excluded. The remaining mean positions were plotted as a histogram (***Figure 11H***) and fit with a single gamma distribution with the median reported. The quality of these gamma distributions and their means were assessed by comparing the gamma model median (the median of the means) to the data median along with R^2.

Row length and branch angles

To determine row lengths and row branch angles visual counting was performed by two viewers on select ROIs of 600 X 600 pixels from each label set. After defining all relevant centroids in the image, a random sample of 5 centroid ROIs per cell were selected with the condition of ROI centers being 600 sub-pixels apart to prevent double counting. These ROIs were overlaid with detected centroid markers and counted for the length of linear rows with a minimum of 3 clusters. A hand selected subset of the randomly picked centroid ROIs was then brightened and used to measure angles in the branched labels to approximately 100 or more angles per label. Angle measures were generated using Fiji ImageJ.

Source Data

All 1D NNMF outputs, NND results, fitting results, and representative raw image files have been deposited at the Federated Research Data Repository and are publicly available. Accession numbers and the DOI are located in ***Supplemental Table 5***. Any further data can be requested from the corresponding author on request. Original MATLAB and R scripts have been deposited at the Federated Research Data Repository, and are publicly available as of the date of publication.

Statistical Analysis

Smoothing of 1D peak intensity data was done using the spline function *spaps* in MATLAB. Smoothing of raw interpeak data was performed using a moving average *smooth* with its default span of 5 in MATLAB. Interpolation of fitted gamma distributions was utilized to calculate central tendency with higher precision than the bin width of the histogram data. Fitting was performed using two methods. NND distributions and isolated peak positions were fitted with a single or dual gamma distribution using the function *lsqnonlin* in MATLAB. All single distribution fits had their model median compared to the data median to determine general error in this method. Error decreased and R^2 increased as θ increased. Interpeak distances from row features were fitted with a damped oscillatory model (Eq 1) iteratively using *lsqnonlin* in MATLAB. Goodness of fit was determined with *gfit2* or internally in functions such as *fit.* To determine if distributions were statistically different we utilized the non-parametric Kosmolgov-Smirnov test in MATLAB. To determine if a single value was likely to belong to a distribution a one-sample t-test was used. Comparisons of two normally distributed datasets were determined with two-sample t-tests or Welch's t-test.

Acknowledgements: We gratefully acknowledge J. Forden for technical assistance, P. Colarusso, C. Brideau, and L. Swift (Live Cell Imaging Facility, Univ. Calgary) for assistance in image calibrations and N.V. Marrion for helpful discussions. This work was supported by a Canadian Institutes for Health Research Operating Grant (R.W.T.), Startup-Research Grant (SERB-SRG; GS), and Natural Science & Engineering Research Council Discovery grant (W.N.). W.N. holds a Canada Research Chair in Computational Neuroscience.

Author Contributions: G.S. and D.G. contributed equally to the work. G.S. prepared fluorophore-tagged constructs, G.S., D.G. and R.W.T. performed dSTORM imaging, G.S., D.G. and W.N. designed data analytics. R.W.T., G.S., D.G. and W.N. wrote the manuscript. R.W.T., G.S. and W.N. supervised the studies.

Figure Legends

Figure 1. IK and Cav1.3 immunolabels exhibit a coordinated pattern of expression in hippocampal neuronal somata.

(**A**-**B**) STORM-TIRF images of immunolabeled clusters for the indicated proteins detected within 150 nm of the membrane surface. A larger field of view (**A**) and magnified ROIs (**B**) reveal a punctate and organized pattern, with IK or Cav1.3 clusters distinguished as rows of clusters on which the alternate label is closely associated or overlaps at discrete intervals (**B,** ROI-1-4, *solid arrows*). Rows of clusters can reach branch points from which one or two rows of clusters extend (**B,** ROI-4, 6, *open arrows*). In other cases IK or Cav1.3 clusters are present in isolation or in close association with the alternate immunolabel **(B,** ROI-5, 7). **(C-E)** NND analysis between clusters in dual labeled cells reveals two populations between similar labels (**C-D**) and a right skewed single peak for IK-Cav1.3 (**E**). (**F-K**) NNMF analysis of dual immunolabels that exhibit fluorescence overlap defines a periodic pattern for cluster rows identified by a damped oscillatory model (**F-H**) or isolated clusters (**I-K**). Unless otherwise indicated, in this and all other figures values for fits (**C-E, I-K**) represent the median of gamma distributions. R^2 values are for the sum of gamma fit distributions (**C-E**), and model periods with R^2 values (**F-H**). Sample values (n) = cells, θ = features. Scale bars: (**A**) 5 µm; (**B**, ROI-1, -2), 1 µm; (**B,** ROI-6), 500 nm; (**B**, ROI-3, 4, 5, and 7), 250 nm. Bin width: (**C-E**) 25 nm, (**F-H**) 15 nm, (**I-K**) 20 nm. In this and subsequent figures, green and red fluorophores were converted to magenta or yellow as indicated (ImageJ). See also ***Supplemental Figure 1 and 2***; ***Supplemental Table 1 and 2***.

Figure 2. RyR2 exhibits a regular pattern of expression in relation to Cav1.3 and IK. (**A-D**) STORM-TIRF images of immunolabeled clusters for the indicated proteins. Larger field views (**A-C**) and magnified ROIs (**B-D**) show that RyR2 clusters exhibit an organized pattern in relation to Cav1.3 (**A-B**) or IK (**C-D**). RyR2 clusters are distributed in rows (**B,** ROI-1, *arrowheads*) that can reach branch points (**B-D,** *open arrows*) or be positioned in isolation. Cav1.3 and IK labels share these patterns and colocalize with RyR2 as rows of clusters (**B,** ROI-1, *arrowheads;* **B** and **D,** ROI-2, *filled arrows*) or as isolated labels. (**E-G**) NND analysis of dual labeled cells reveals two populations of distance between RyR2 clusters (**E**) and right-skewed single peaks for RyR2-Cav1.3 (**F**) or RyR2-IK (**G**). (**H-M**) NNMF analysis defines a periodic pattern for colabeled cluster rows (**H-J**) or a single distribution for isolated clusters (**K-M**). Sample values (n) = cells, θ = features. Calibration bars: (**A-C**) 5 µm; (**B-D**) 2 µm. Bin widths: (**E-G)** 25 nm, (**H-J**) 15 nm, (**K-M**) 20 nm. See also ***Supplemental Figure 1-3, Supplemental Table 1 and 2.***

Figure 3. Spectrin βII exhibits a structured pattern associated with Cav1.3. (**A-D**) STORM-TIRF images of immunolabeled clusters for the indicated proteins. Shown are larger fields of view for a cell labeled for spectrin βII (**A** and **B**) and the same cell dual labeled for spectrin βII and Cav1.3 (**C** and **D**). ROIs are magnified in (**B** and **D**), with the same frame of view in (**B,** ROI-2) and (**D,** ROI-1). (**B** and **D**) Spectrin βII labeled clusters organize as rows of clusters (*arrowheads*) that extend to branch points (*open arrows*) or as isolated clusters (*filled arrows*). Dual labeling reveals Cav1.3 clusters that overlap with spectrin βII cluster rows (**C** and **D,** ROI-1, 2, *arrowheads*). (**E-F**) NND in dual labeled cells reveals two populations between spectrin βII clusters (**E**) and one for spectrin βII-Cav1.3 (**F**). (**G-J**) NNMF analysis

defines a periodic pattern for cluster rows (**G** and **H**) or a single distribution for isolated clusters (**I** and **J**). Sample values (n) = cells, θ = features. R^2 value in (**E**) corresponds to the superimposed combined fit for the two populations. Scale bars: (**A** and **C**) 5 µm; (**B,** ROI-1, -2; **D,** ROI-1), 2 µm; (**D,** ROI-2), 500 nm. Bin widths: (**E-F)** 25 nm, (**G-H**) 15 nm, (**I-J**) 20 nm. See also ***Supplemental Table 1 and 2.***

Figure 4. Spectrin exhibits an organized pattern that is closely associated with IK and RyR2 distributions. (**A-D**) STORM-TIRF images of immunolabeled clusters for the indicated proteins. Larger field views (**A** and **C**) with ROIs magnified (**B** and **D**) identify rows of spectrin βII clusters that can reach branch points (*open arrows*) that colocalize or alternate with rows of IK or RyR2 (*arrowheads*). Isolated clusters can be distinguished for IK or RyR2 (**B,** ROI-2, **D**, ROI-1, 2; *filled arrows*). (**E-F**) NND analysis between IK-spectrin βII (**E**) and RyR2-spectrin βII (**F**).

(**G-J**), NNMF analysis defines a periodic pattern for cluster rows (**G-H**) or a single distribution for isolated clusters (**I-J**). Sample values (n) = cells, θ = features. Scale bars: (**A** and **C**) 5 µm; **(B** and **D**, ROI-1, -2), 1 µm. Bin widths: (**E-F)** 25 nm, (**G-H**) 15 nm, (**I-J**) 20 nm. See also ***Supplemental Figure 3, Supplemental Table 1 and 2***.

Figure 5. Actinin I and actinin II exhibit an organized pattern in relation to spectrin βII. (**A-D**) STORM-TIRF images of immunolabeled clusters for the indicated proteins. Shown are dual labeled images for spectrin with actinin I (**A-B**) or with actinin II (**C-D**), with ROIs magnified in (**B** and **D**). Rows of spectrin βII or actinin clusters can extend to branch points (*open arrows*), colocalize (*solid arrows*), or alternate to extend or bridge rows of labels (*arrowheads*).

(**E-F**) NND analysis between actinin I-spectrin βII (**E**) and actinin II-spectrin βII (**F**).

(**G-J**) NNMF analysis defines a periodic pattern for cluster rows (**G-H**) or a single distribution for isolated clusters (**I-J**). Sample values (n) = cells, θ = features. Scale bars: (**A** and **C**) 5 µm; (**B** and **D,** ROI-1, 2), 1 µm; (**B** and **D,** lower ROIs), 200 nm. Bin widths: (**E-F**) 25 nm, (**G-H**) 15 nm, (**I-J**) 20 nm. See also ***Supplemental Figure 4, Supplemental Table 1 and 2.***

Figure 6. Actinin I and actinin II distributions are aligned with CaRyK complex proteins. (**A-F**) STORM-TIRF images of immunolabeled clusters for the indicated proteins. Shown are dual labeled images for the indicated CaRyK complex proteins and actinin isoforms. Larger field views (**A, C, E**) and associated ROIs (**B, D, F**) identify clusters that align in rows that either overlap or alternate (*arrowheads*) with actinin isoforms. Cluster rows can extend to branch points (*open arrows*), colocalize (*solid arrows*), or alternate to extend or bridge rows of labels (*arrowheads*). (**G-I**) NND analysis between actinin I - Cav1.3 (**G**), actinin II - IK (**H**) and actinin II - RyR2 (**I**). **(J-O**) NNMF analysis defines a periodic pattern for cluster rows (**J-L**) or a single distribution for isolated clusters (**M-O**). Sample values (n) = cells, θ = features. Scale bars: (**A, C, E**) 5 µm; (**B, D, F**), 1 µm. Bin widths: (**G-I)** 25 nm, (**J-L**) 15 nm, (**M-O**) 20 nm. See also ***Supplemental Table 1 and 2.***

Figure 7. Correspondence between the spatial organization of CaRyK complex proteins and spectrin. (**A**) Plots of the percent of clusters aligned in rows of at least three clusters for the indicated immunolabels. (**B**) Plots of the angles at branch points of cluster rows for the indicated immunolabels. Bin widths: 5 degrees. (**C-J**) Comparison of model fits for cluster rows (**C-F**) and fits for isolated clusters (**G-**

J) for the indicated pairs of immunolabels. The damped oscillatory models are amplitude and phase shift normalized for comparison (first crest of fit, 0 nm) (**C-F**) and gamma model centers are amplitude normalized (**G-J**). Gaussian fits are used for plots in (**B**) and average values are mean ± SEM. Fits in (**C-E**) are from ***Supplemental Figure 1-4, Supplemental Table 1-4.***

Figure 8. The use of NNMF to define patterns in immunolabeled cluster centroids. (**A-C**) Procedure to define relationships between immunolabeled clusters in representative STORM-TIRF images of neuronal processes outside of the soma labeled for spectrin βII. A systematic pixel-by-pixel search identifies the center of a detected centroid (**A,** *cross*) for spectrin βII labeling. Images are then rotated to a position where its nearest neighboring centroid is oriented to the left and the ROI is stored for feature detection (**B-C**). Below the images in (**B-C**) are 1D displays of normalized pixel intensity aligned with the profile indicated by *dashed lines* for a row of clusters consistent with the MPS (**A-B**) as well as isolated clusters (**C**). (**D**) NND analysis of spectrin βII clusters in neuronal processes reveal two populations of inter cluster distances, with the majority fitting a distribution with a median value of 144 nm. (**E**) Representative example of centroid features extracted by NNMF from spectrin βII labeled neural processes outside the soma of a single cell with k = 6. *Vertical lines* denote detected peak positions. (**F-G**) Two representative examples of features containing rows (**F**) or isolated clusters (**G**) for spectrin βII labeling. Scale bars: (**A-C**) 500 nm. Bin width (**D**) 25 nm.

Figure 9: Rationale for feature number selection for NNMF. The effects of using different numbers of features (k) to calculate the distance between rows of clusters using NNMF. NNMF generates features as rows of a matrix which are reported in decreasing importance to the original data set. Every cluster centroid image prior to input into NNMF has a central point spread function upon which the image is aligned to identify intercluster distances of neighboring rows of clusters. (**A**) A representative case of feature detection for different k values for spectrin βII images, with each case illustrating the third feature calculated by NNMF. ROIs of the regions indicated by a *white box* are shown expanded above. As k increases, attributes of each feature become diluted until the central centroid (*white* arrows) becomes diminished or is no more prominent than noise (i.e. k = 8). (**B**) Scatter plot showing a progressive loss of central centroids in downstream analysis as the number of features generated is increased. *Red dashed line* indicates k = 6 (portion = 0.8333). (**C**) Box plot of the portion of features across CaRyK, spectrin and actinin datasets which contain a detectable central centroid to calculate intercluster distances in rows of immunolabeled clusters (mean = 0.824 ± 0.0075). Analyses were conducted with k = 6 to avoid instances where the centering centroid was miniscule or absent and ensure that features reflected a plausible centroid image while maximizing the number of features for downstream analysis. (**D**) Representative example of the top six features extracted for spectrin βII in MAP2 positive or negative processes of hippocampal cells. Scale bars: (**A**, ROIs) 300 nm, (**D**) 300 nm. Sample values (n) in (**C**) reflect all data sets for CaRyK, spectrin and actinin immunolabels.

Figure 10. Comparison of periodicity in cluster organization measured by autocorrelation vs NNMF. (**A-B**) Representative STORM-TIRF image of spectrin βII labeling with an overlaid larger field image of MAP2-GFP labeling (**A**). Two processes are highlighted as MAP2 negative putative axons

(ROI-1) and MAP2 positive putative dendrites (ROI-2) (**B**). (**C-D**) Spectrin βII labeling of MAP2 negative or MAP2 positive processes outside of the soma are analyzed for periodicity by autocorrelation (**C**) or NNMF (**D**). In (**C**) the autocorrelations (*blue lines*) and normalized derivatives (*magenta lines*) are shown superimposed and drawn from the specific ROI examples in (**B**), while mean periods are calculated from the entire population of clusters. In (**D**) histograms of interpeak distance of row classified spectrin βII features from the same data set are shown superimposed with the damped oscillatory model fits (*red lines*) calculated by NNMF. Scale bars: (**A**) 5 µm, (**A**, inset ROI-1,2) 500 nm, (**B,** ROI-1, 2) 300 nm. Average values are mean ± SEM. Sample values (n) = cells, θ = NNMF row features (**E**). Bin widths: (**D**) 15.4 nm.

Figure 11. Defining inter cluster distances from NNMF. Procedure for oscillatory model fitting of the NNMF defined interpeak distance histograms. (**A**) Plot of the heights of binned interpeak distances of the initial 3 cycles of row classified features generated by NNMF of spectrin βII labeled processes. Interpeak distances are cropped to a range of 15-70 sub-pixels to accommodate the highest S/N region. Shown superimposed is data before and after smoothing with a moving average to improve model fit. (**B**) Superimposed records of smoothed data trace from (**A**) fit with a damped oscillatory model for 4 iterations using a least-squares method. (**C-E**) Representative example of best fit model and error values for spectrin βII NNMF calculations in processes, with the best fit model (*black line*) superimposed on the histogram of raw interpeak distance data in (**C**). Shown in (**D-E**) is the histogram of error between model and data (**D**), with error distributed around zero. A scatter plot of error along the X axis of data in (**C**) is relatively homoscedastic (**E**). (**F-H**) Procedure for defining peak centers of isolated features identified by NNMF. A representative example of an isolated classified feature as a plot of probability in relation to distance from centering centroid for spectrin βII - spectrin βII (**F**). An examination window of -1504 to -367 nm (*gray dashed lines*) is used to avoid the influence of the centering centroid or distant data tails in defining the peak of isolated clusters (*magenta vertical line*) (**F**). (**G**) Data within the examination window is fit with a single gaussian. A plot of the mean and SD of fits of isolated cluster gaussians is used to confirm a single population of gaussians and eliminate outliers defined using *rmoutliers*. Any gaussians that fell outside of the examination window (*gray dashed lines*) were removed, along with gaussians that were not well fit to the data they represented ($R^2 \leq 0.9$). (**H**) Final histogram of accepted means for isolated cluster distances determined in (**F-G**). Bin widths: (**C**) 15 nm, (**D**) 0.04, (**H**) 20 nm.

Supplemental Figure 1. The spatial distribution of CaRyK complex immunolabeled clusters at the soma is not random. Related to ***Figure 1 and 2***. (**A-C**) *Left column* provides NND distributions of the indicated CaRyK complex proteins. *Right column* indicates NND distributions for the same datasets after randomizing centroid positions. Significant differences exist between experimental and randomized data for each protein (non-parametric 2- sample Kolmogorov–Smirnov test (KS)): (**A**) $p < 0.001$, KS-stat = 0.1180; (**B**) $p < 0.001$, KS-stat = 0.1999; (**C**) $p < 0.001$, KS-stat = 0.1957). Numerical indicators adjacent to histograms represent median values. Sample values (n) = cells, ρ, number of centroids detected across all images for a given label set. Bin widths: (**A-C**) 25 nm.

Supplemental Figure 2. Related to *Figure 1 and 2.* Generating images of fluorescent emission overlap for NNMF analysis. Related to Figures 1-6. (**A-C**) Larger field views of hippocampal neurons dual immunolabeled for the indicated proteins. (**D-F**) Expanded views of ROIs from images in (**A-C**) illustrating overlap of some fluorescence emissions (white chroma, *arrows*) suggestive of protein colocalizations. (**G-I**) Black and white images of overlap-dependent intensity representations of the dual labels in (**D-F)** to apply NNMF on dual labeled clusters. Pixel intensity of the overlap image is determined pixel wise by: $Overlap_{xy} = \sqrt{(Green\ Intensity_{xy})(Red\ Intensity_{xy})}$.
Scale bars: (**A-C**) 5 µm; (**D-I**), 500 nm. See also ***Supplemental Table 4.***

Supplemental Figure 3. Spectrin βII clusters distribute with similar patterns as IK and RyR2. *Related to Figure 3 and 4.* (**A-D**) NND histograms of similar immunolabels in two sets of dual labeled tissue (**A-B,** spectrin βII-RyR2; **C-D,** spectrin βII-IK) reveals populations that can be described by two gamma fits. Values are the median of fit gamma distributions and R^2 of the combined fits. Sample values (n) represent the number of individual cells analyzed. Bin widths: 25 nm.

Supplemental Figure 4. Actinin I and actinin II immunolabels exhibit a structured pattern indicative of rows and isolated clusters. Related to *Figure 5.* (**A-B**) NND analysis within actinin I clusters (**A**) and actinin II clusters (**B**) reveal two populations of inter-centroid distance fit with two gamma distributions. Distributions are comparable to that of spectrin βII (see **Figs. 3 and S7**). (**C-F**) NNMF analysis of the indicated immunolabels defines a regular periodicity of cluster rows (**C-D**) or isolated clusters (**E-F**). Medians of gamma distributions, R^2 values of fitted gamma distributions (**A, B, E,** and **F**), model periods and with their associated R^2 values (**C-D**) are indicated on plots. Total number of centroids detected to apply NNMF (**C-F**): actinin I-actinin I, 19,767; actinin II-actinin II, 21,634. Sample values (n)= cells, Θ = features. Bin widths: (**A-B)** 25 nm, (**C-D**) 15 nm, (**E-F**) 20 nm.

Supplemental Table 1. Summary comparisons of fitted gamma mixture models on NND for the indicated protein pairs. All cells were imaged with two immunolabel targets and nearest neighbor distance (NND) distributions calculated for all clusters. NND was calculated using LAMA's morphological cluster analysis and fitted with a mixed gamma model to define central tendency for each gamma distribution in the NND histograms of ***Figure 1-6.*** Cluster pairs = the labeled targets which are being compared to generate the NND histogram. n = the number of cells. R^2 = coefficient of determination when comparing the sum of fitted gamma distributions to the NND histogram. GMM = gamma-mixture model.

Supplemental Table 2. Summary of NNMF feature analysis for the indicated protein pairs. Information about data entered into the NNMF workflow and the results. n = the number of cells imaged. Centroids = the sum of weighted positions across all images that were assessed by NNMF to generate features. Θ = the number of features generated per label set. Row Cluster Data = features from NNMF which were assessed for peak density anticipated in regular and repeating clusters. Isolated Cluster Data = features from NNMF which were assessed with a low peak density anticipated by isolated centroids. Period = period of fitted damped oscillatory model on interpeak data from features. R^2 = coefficient of determination when comparing data to the fitted model. SSQ = sum of squared error between smoothed

interpeak data and the fitted model. Median center = displacement of fitted gamma on isolated features from their reference position. Empty cells represent instances where no interpretable data was produced.

Supplemental Table 3. The distribution of cluster row branchpoint angles are not significantly different. With sample size > 100 normality assumption was ignored and Welch 2 sample t-test was used to compare the central tendency of distributions. Two sample Kolmogorov-smirnov (KS) test was used to test the null hypothesis of the distributions being from the same population. Statistical calculations were completed using R software. df, degrees of freedom. See also ***Figure 7B***.

Supplemental Table 4. Percent overlap of pixels labeled for CaRyK complex proteins. Dual labeled images were masked to their ROIs, thresholded at > 20% maximal intensity and all pixels were counted. When pixels in the same position in both channels were greater than the threshold, they were counted as overlapped and divided by the sum of pixels greater than threshold in each channel. Calculated in MATLAB with custom scripts.

Supplemental Table 5. List of reagents and supplies used, software applications, and location of data repository.

References

Antonucci DE, Lim ST, Vassanelli S, Trimmer JS. 2001. Dynamic localization and clustering of dendritic Kv2.1 voltage-dependent potassium channels in developing hippocampal neurons. *Neuroscience* **108**:69–81.

Berry MW, Browne M, Langville AN, Pauca VP, Plemmons RJ. 2007. Algorithms and applications for approximate nonnegative matrix factorization. *Comput Stat Data Anal* **52**:155–173.

Brown JW, Bullitt E, Sriswasdi S, Harper S, Speicher DW, McKnight CJ. 2015. The Physiological Molecular Shape of Spectrin: A Compact Supercoil Resembling a Chinese Finger Trap. *PLoS Comput Biol* **11**:e1004302.

D'Este E, Kamin D, Balzarotti F, Hell SW. 2017. Ultrastructural anatomy of nodes of Ranvier in the peripheral nervous system as revealed by STED microscopy. *Proc Natl Acad Sci U S A* **114**:E191–E199.

D'Este E, Kamin D, Göttfert F, El-Hady A, Hell SW. 2015. STED nanoscopy reveals the ubiquity of subcortical cytoskeleton periodicity in living neurons. *Cell Rep* **10**:1246–1251.

D'Este E, Kamin D, Velte C, Göttfert F, Simons M, Hell SW. 2016. Subcortical cytoskeleton periodicity throughout the nervous system. *Sci Rep* **6**:22741.

Deutsch E, Weigel AV, Akin EJ, Fox P, Hansen G, Haberkorn CJ, Loftus R, Krapf D, Tamkun MM. 2012. Kv2.1 cell surface clusters are insertion platforms for ion channel delivery to the plasma membrane. *Mol Biol Cell* **23**:2917–2929.

Dixon RE, Trimmer JS. 2023. Endoplasmic Reticulum-Plasma Membrane Junctions as Sites of Depolarization-Induced Ca2+ Signaling in Excitable Cells. *Annu Rev Physiol*. doi:10.1146/annurev-physiol-032122-104610

Engbers JD, Anderson D, Asmara H, Rehak R, Mehaffey WH, Hameed S, McKay BE, Kruskic M, Zamponi GW, Turner RW. 2012. Intermediate conductance calcium-activated potassium channels modulate summation of parallel fiber input in cerebellar Purkinje cells. *Proc Natl Acad Sci U S A* **109**:2601–2606.

Fox PD, Haberkorn CJ, Akin EJ, Seel PJ, Krapf D, Tamkun MM. 2015. Induction of stable ER–plasma-membrane junctions by Kv2.1 potassium channels. *J Cell Sci* **128**:2096–2105.

Fu J, Dai X, Plummer G, Suzuki K, Bautista A, Githaka JM, Senior L, Jensen M, Greitzer-Antes D, Manning Fox JE, Gaisano HY, Newgard CB, Touret N, MacDonald PE. 2017. Kv2.1 Clustering Contributes to Insulin Exocytosis and Rescues Human β-Cell Dysfunction. *Diabetes* **66**:1890–1900.

Gao Y, Perkins EM, Clarkson YL, Tobia S, Lyndon AR, Jackson M, Rothstein JD. 2011. β-III spectrin is critical for development of purkinje cell dendritic tree and spine morphogenesis. *J Neurosci* **31**:16581–16590.

Grum VL, Li D, MacDonald RI, Mondragón A. 1999. Structures of two repeats of spectrin suggest models of flexibility. *Cell* **98**:523–535.

Hall DD, Dai S, Tseng P-Y, Malik Z, Nguyen M, Matt L, Schnizler K, Shephard A, Mohapatra DP, Tsuruta F, Dolmetsch RE, Christel CJ, Lee A, Burette A, Weinberg RJ, Hell JW. 2013. Competition between α-actinin and Ca2 -Calmodulin Controls Surface Retention of the L-type Ca2 Channel CaV1.2. *Neuron*. doi:10.1016/j.neuron.2013.02.032

Han B, Zhou R, Xia C, Zhuang X. 2017. Structural organization of the actin-spectrin–based membrane skeleton in dendrites and soma of neurons. *Proc Natl Acad Sci U S A* **114**:E6678–E6685.

He J, Zhou R, Wu Z, Carrasco MA, Kurshan PT, Farley JE, Simon DJ, Wang G, Han B, Hao J, Heller E, Freeman MR, Shen K, Maniatis T, Tessier-Lavigne M, Zhuang X. 2016. Prevalent presence of periodic actin–spectrin-based membrane skeleton in a broad range of neuronal cell types and animal species. *Proc Natl Acad Sci U S A* **113**:6029–6034.

Hiess F, Vallmitjana A, Wang R, Cheng H, ter Keurs HEDJ, Chen J, Hove-Madsen L, Benitez R, Chen SRW. 2015. Distribution and Function of Cardiac Ryanodine Receptor Clusters in Live Ventricular Myocytes. *J Biol Chem* **290**:20477–20487.

Higham J, Sahu G, Wazen R-M, Colarusso P, Gregorie A, Harvey BSJ, Goudswaard L, Varley G, Sheppard DN, Turner RW, Marrion NV. 2019. Preferred Formation of Heteromeric Channels between Coexpressed SK1 and IKCa Channel Subunits Provides a Unique Pharmacological Profile of Ca2 -Activated Potassium Channels. *Molecular Pharmacology*. doi:10.1124/mol.118.115634

Huang CY-M, Zhang C, Ho TS-Y, Oses-Prieto J, Burlingame AL, Lalonde J, Noebels JL, Leterrier C, Rasband MN. 2017. αII Spectrin Forms a Periodic Cytoskeleton at the Axon Initial Segment and Is Required for Nervous System Function. *J Neurosci* **37**:11311–11322.

Johnson B, Leek AN, Tamkun MM. 2019. Kv2 channels create endoplasmic reticulum / plasma membrane junctions: a brief history of Kv2 channel subcellular localization. *Channels* **13**:88–101.

King B, Rizwan AP, Asmara H, Heath NC, Engbers JD, Dykstra S, Bartoletti TM, Hameed S, Zamponi GW, Turner RW. 2015. IKCa channels are a critical determinant of the slow AHP in CA1 pyramidal neurons. *Cell Rep* **11**:175–182.

Leung YM, Kang Y, Gao X, Xia F, Xie H, Sheu L, Tsuk S, Lotan I, Tsushima RG, Gaisano HY. 2003. Syntaxin 1A binds to the cytoplasmic C terminus of Kv2.1 to regulate channel gating and trafficking. *J Biol Chem* **278**:17532–17538.

Liem RKH. 2016. Cytoskeletal Integrators: The Spectrin Superfamily. *Cold Spring Harb Perspect Biol* **8**. doi:10.1101/cshperspect.a018259

Lim ST, Antonucci DE, Scannevin RH, Trimmer JS. 2000. A novel targeting signal for proximal clustering of the Kv2.1 K+ channel in hippocampal neurons. *Neuron* **25**:385–397.

Lorenzo DN, Edwards RJ, Slavutsky AL. 2023. Spectrins: molecular organizers and targets of neurological disorders. *Nat Rev Neurosci*. doi:10.1038/s41583-022-00674-6

Lukinavičius G, Reymond L, D'Este E, Masharina A, Göttfert F, Ta H, Güther A, Fournier M, Rizzo S, Waldmann H, Blaukopf C, Sommer C, Gerlich DW, Arndt H-D, Hell SW, Johnsson K. 2014. Fluorogenic probes for live-cell imaging of the cytoskeleton. *Nat Methods* **11**:731–733.

Lu L, Timofeyev V, Li N, Rafizadeh S, Singapuri A, Harris TR, Chiamvimonvat N. 2009. Alpha-actinin2 cytoskeletal protein is required for the functional membrane localization of a Ca2+-activated K+ channel (SK2 channel). *Proc Natl Acad Sci U S A* **106**:18402–18407.

Lu L, Zhang Q, Timofeyev V, Zhang Z, Young JN, Shin H-S, Knowlton AA, Chiamvimonvat N. 2007. Molecular coupling of a Ca2+-activated K+ channel to L-type Ca2+ channels via alpha-actinin2. *Circ Res* **100**:112–120.

Lux SE 4th. 2016. Anatomy of the red cell membrane skeleton: unanswered questions. *Blood* **127**:187–199.

Machnicka B, Grochowalska R, Bogusławska DM, Sikorski AF, Lecomte MC. 2012. Spectrin-based skeleton as an actor in cell signaling. *Cell Mol Life Sci* **69**:191–201.

Malkusch S, Heilemann M. 2016. Extracting quantitative information from single-molecule super-resolution imaging data with LAMA - LocAlization Microscopy Analyzer. *Sci Rep* **6**:34486.

Mandikian D, Bocksteins E, Parajuli LK, Bishop HI, Cerda O, Shigemoto R, Trimmer JS. 2014. Cell type-specific spatial and functional coupling between mammalian brain Kv2.1 K+ channels and ryanodine receptors. *J Comp Neurol* **522**:3555–3574.

Marek R, Caruso M, Rostami A, Grinspan JB, Das Sarma J. 2008. Magnetic cell sorting: a fast and effective method of concurrent isolation of high purity viable astrocytes and microglia from neonatal mouse brain tissue. *J Neurosci Methods* **175**:108–118.

Maverick EE, Tamkun MM. 2022. High spatial density is associated with non-conducting Kv channels from two families. *Biophys J* **121**:755–768.

Moore SJ, Murphy GG. 2020. The role of L-type calcium channels in neuronal excitability and aging. *Neurobiol Learn Mem* **173**:107230.

Nans A, Mohandas N, Stokes DL. 2011. Native ultrastructure of the red cell cytoskeleton by cryo-electron tomography. *Biophys J* **101**:2341–2350.

Rentsch J, Bandstra S, Sezen B, Sigrist P, Bottanelli F, Schmerl B, Shoichet S, Noé F, Sadeghi M, Ewers H. 2024. Sub-membrane actin rings compartmentalize the plasma membrane. *J Cell Biol* **223**. doi:10.1083/jcb.202310138

Sadeghi A, Doyle AD, Johnson BD. 2002. Regulation of the cardiac L-type Ca2+ channel by the actin-binding proteins alpha-actinin and dystrophin. *Am J Physiol Cell Physiol* **282**:C1502–11.

Sahu G, Asmara H, Zhang FX, Zamponi GW, Turner RW. 2017. Activity-Dependent Facilitation of CaV1.3 Calcium Channels Promotes KCa3.1 Activation in Hippocampal Neurons. *J Neurosci* **37**:11255–11270.

Sahu G, Turner RW. 2021. The molecular basis for the calcium-dependent sAHP in CA1 hippocampal pyramidal cells. *Front Physiol* **1**:1–25.

Sahu G, Wazen R-M, Colarusso P, Chen SRW, Zamponi GW, Turner RW. 2019. Junctophilin Proteins Tether a Cav1-RyR2-KCa3.1 Tripartite Complex to Regulate Neuronal Excitability. *Cell Reports* **28**:2427–2442.e6.

Tedoldi A, Ludwig P, Fulgenzi G, Takeshima H, Pedarzani P, Stocker M. 2020. Calcium-induced calcium release and type 3 ryanodine receptors modulate the slow afterhyperpolarising current, sIAHP, and its potentiation in hippocampal pyramidal neurons. *PLoS One* **15**:e0230465.

Tiwari MN, Mohan S, Biala Y, Shor O, Benninger F, Yaari Y. 2022. Corticotropin Releasing Factor Mediates KCa3.1 Inhibition, Hyperexcitability, and Seizures in Acquired Epilepsy. *J Neurosci* **42**:5843–5859.

Tiwari MN, Mohan S, Biala Y, Yaari Y. 2019. Protein kinase A-mediated suppression of the slow afterhyperpolarizing KCa3.1 current in temporal lobe epilepsy. *J Neurosci*. doi:10.1523/JNEUROSCI.1603-19.2019

Trimmer JS. 2015. Subcellular localization of K+ channels in mammalian brain neurons: remarkable precision in the midst of extraordinary complexity. *Neuron* **85**:238–256.

Turner M, Anderson DE, Bartels P, Nieves-Cintron M, Coleman AM, Henderson PB, Man KNM, Tseng P-Y, Yarov-Yarovoy V, Bers DM, Navedo MF, Horne MC, Ames JB, Hell JW. 2020. α-Actinin-1 promotes activity of the L-type Ca2+ channel Cav 1.2. *EMBO J* **39**:e102622.

Turner RW, Asmara H, Engbers JDT, Miclat J, Rizwan AP, Sahu G, Zamponi GW. 2016. Assessing the role of IKCa channels in generating the sAHP of CA1 hippocampal pyramidal cells. *Channels* **10**:313–319.

Unsain N, Stefani FD, Cáceres A. 2018. The Actin/Spectrin Membrane-Associated Periodic Skeleton in Neurons. *Front Synaptic Neurosci* **10**:10.

Vegas-Sánchez-Ferrero G, Martín-Fernández M, Sanches JM. 2014. A Gamma Mixture Model for IVUS Imaging In: Saba L, Sanches JM, Pedro LM, Suri JS, editors. Multi-Modality Atherosclerosis Imaging and Diagnosis. New York, NY: Springer New York. pp. 155–171.

Vierra NC, Kirmiz M, van der List D, Santana LF, Trimmer JS. 2019. Kv2.1 mediates spatial and functional coupling of L-type calcium channels and ryanodine receptors in mammalian neurons. *Elife* **8**. doi:10.7554/eLife.49953

Vierra NC, O'Dwyer SC, Matsumoto C, Santana LF, Trimmer JS. 2021. Regulation of neuronal excitation-transcription coupling by Kv2.1-induced clustering of somatic L-type Ca2+ channels at ER-PM junctions. *Proc Natl Acad Sci U S A* **118**. doi:10.1073/pnas.2110094118

Vierra NC, Trimmer JS. 2022. Ion Channel Partnerships: Odd and Not-So-Odd Couples Controlling Neuronal Ion Channel Function. *Int J Mol Sci* **23**. doi:10.3390/ijms23041953

Wang K, Mateos-Aparicio P, Honigsperger C, Raghuram V, Wu WW, Ridder MC, Sah P, Maylie J, Storm JF, Adelman JP. 2016. IK1 channels do not contribute to the slow afterhyperpolarization in pyramidal neurons. *Elife* **5**:e11206.

Wang Y-X, Zhang Y-J. 2013. Nonnegative Matrix Factorization: A Comprehensive Review. *IEEE Trans Knowl Data Eng* **25**:1336–1353.

Xu K, Zhong G, Zhuang X. 2013. Actin, spectrin, and associated proteins form a periodic cytoskeletal structure in axons. *Science* **339**:452–456.

Zhong G, He J, Zhou R, Lorenzo D, Babcock HP, Bennett V, Zhuang X. 2014. Developmental mechanism of the periodic membrane skeleton in axons. *Elife* **3**. doi:10.7554/eLife.04581

Zhou R, Han B, Nowak R, Lu Y, Heller E, Xia C, Chishti AH, Fowler VM, Zhuang X. 2022. Proteomic and functional analyses of the periodic membrane skeleton in neurons. *Nat Commun* **13**:3196.

Zuccotti A, Clementi S, Reinbothe T, Torrente A, Vandael DH, Pirone A. 2011. Structural and functional differences between L-type calcium channels: crucial issues for future selective targeting. *Trends Pharmacol Sci* **32**:366–375.

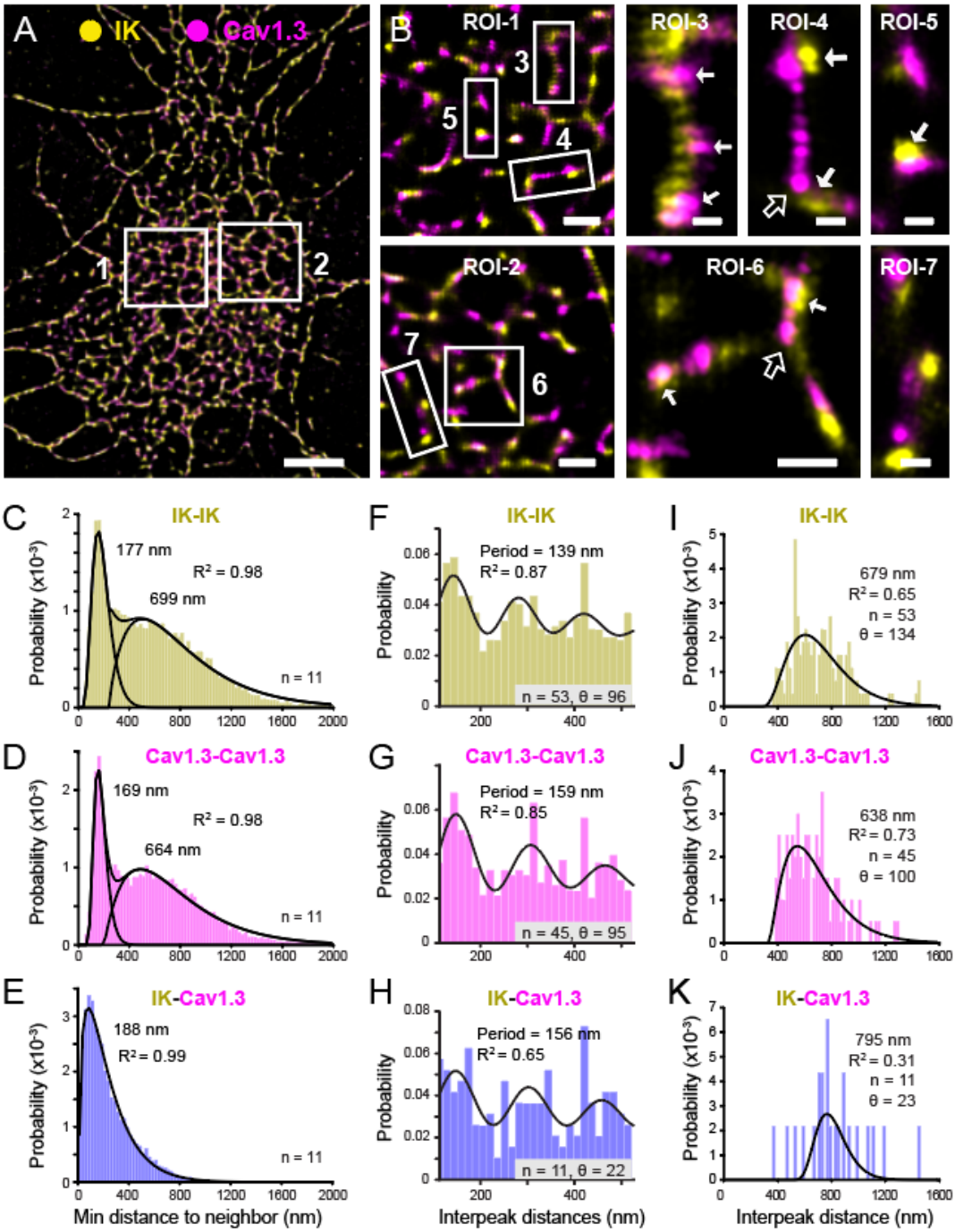

Figure 1. IK and Cav1.3 immunolabels exhibit a coordinated pattern of expression in hippocampal neuronal somata.

(**A-B**) STORM-TIRF images of immunolabeled clusters for the indicated proteins detected within 150 nm of the membrane surface. A larger field of view (**A**) and magnified ROIs (**B**) reveal a punctate and organized pattern, with IK or Cav1.3 clusters distinguished as rows of clusters on which the alternate label is closely associated or overlaps at discrete intervals (**B,** ROI-1-4, *solid arrows*). Rows of clusters can reach branch points from which one or two rows of clusters extend (**B,** ROI-4, 6, *open arrows*). In other cases IK or Cav1.3 clusters are present in isolation or in close association with the alternate immunolabel (**B,** ROI-5, 7). **(C-E)** NND analysis between clusters in dual labeled cells reveals two populations between similar labels (**C-D**) and a right skewed single peak for IK-Cav1.3 (**E**). (**F-K**) NNMF analysis of dual immunolabels that exhibit fluorescence overlap defines a periodic pattern for cluster rows identified by a damped oscillatory model (**F-H**) or isolated clusters (**I-K**). Unless otherwise indicated, in this and all other figures values for fits (**C-E, I-K**) represent the median of gamma distributions. R^2 values are for the sum of gamma fit distributions (**C-E**), and model periods with R^2 values (**F-H**). Sample values (n) = cells, θ = features. Scale bars: (**A**) 5 µm; (**B**, ROI-1, -2), 1 µm; (**B,** ROI-6), 500 nm; (**B**, ROI-3, 4, 5, and 7), 250 nm. Bin width: (**C-E**) 25 nm, (**F-H**) 15 nm, (**I-K**) 20 nm. In this and subsequent figures, green and red fluorophores were converted to magenta or yellow as indicated (ImageJ). See also ***Supplemental Figure 1 and 2***; ***Supplemental Table 1 and 2***.

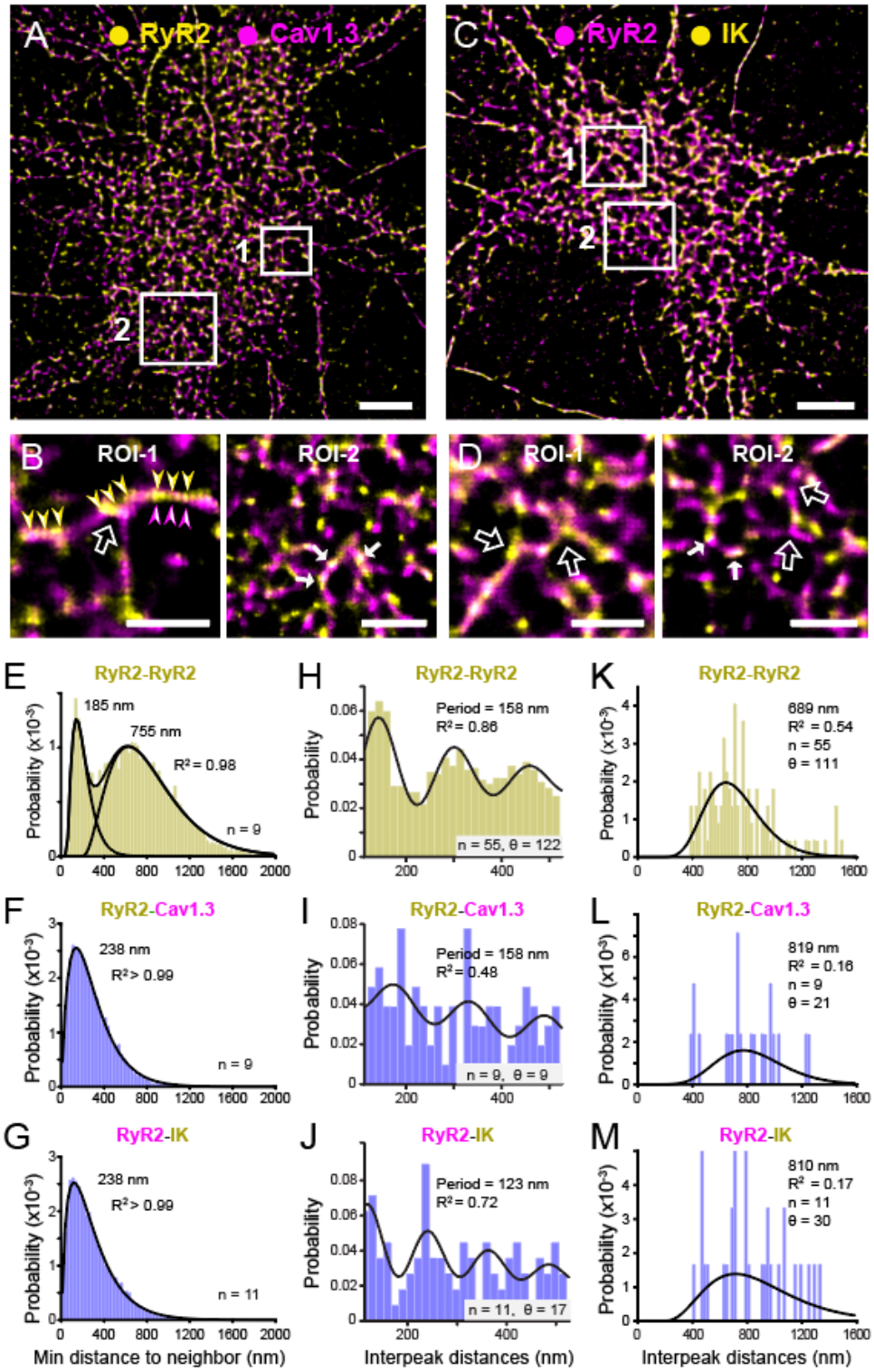

Figure 2. RyR2 exhibits a regular pattern of expression in relation to Cav1.3 and IK. (**A-D**) STORM-TIRF images of immunolabeled clusters for the indicated proteins. Larger field views (**A-C**) and magnified ROIs (**B-D**) show that RyR2 clusters exhibit an organized pattern in relation to Cav1.3 (**A-B**) or IK (**C-D**). RyR2 clusters are distributed in rows (**B,** ROI-1, *arrowheads*) that can reach branch points (**B-D,** *open arrows*) or be positioned in isolation. Cav1.3 and IK labels share these patterns and colocalize with RyR2 as rows of clusters (**B,** ROI-1, *arrowheads;* **B** and **D,** ROI-2, *filled arrows*) or as isolated labels. (**E-G**) NND analysis of dual labeled cells reveals two populations of distance between RyR2 clusters (**E**) and right-skewed single peaks for RyR2-Cav1.3 (**F**) or RyR2-IK (**G**). (**H-M**) NNMF analysis defines a periodic pattern for colabeled cluster rows (**H-J**) or a single distribution for isolated clusters (**K-M**). Sample values (n) = cells, θ = features. Calibration bars: (**A-C**) 5 µm; (**B-D**) 2 µm. Bin widths: (**E-G**) 25 nm, (**H-J**) 15 nm, (**K-M**) 20 nm. See also ***Supplemental Figure 1-3, Supplemental Table 1 and 2.***

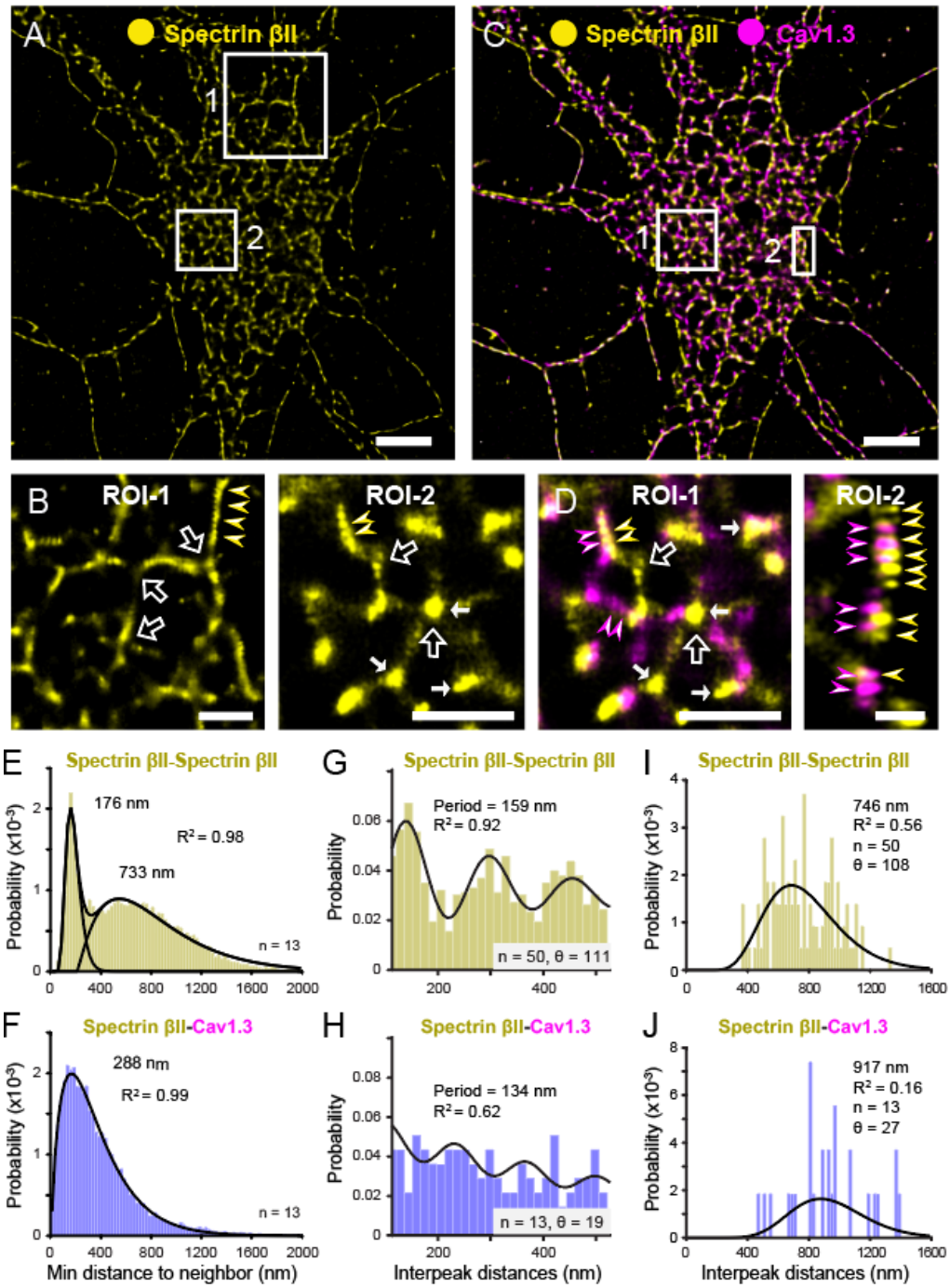

Figure 3. Spectrin βII exhibits a structured pattern associated with Cav1.3. (**A-D**) STORM-TIRF images of immunolabeled clusters for the indicated proteins. Shown are larger fields of view for a cell labeled for spectrin βII (**A** and **B**) and the same cell dual labeled for spectrin βII and Cav1.3 (**C** and **D**). ROIs are magnified in (**B** and **D**), with the same frame of view in (**B,** ROI-2) and (**D,** ROI-1). (**B** and **D**) Spectrin βII labeled clusters organize as rows of clusters (*arrowheads*) that extend to branch points (*open arrows*) or as isolated clusters (*filled arrows*). Dual labeling reveals Cav1.3 clusters that overlap with spectrin βII cluster rows (**C** and **D,** ROI-1, 2, *arrowheads*). (**E-F**) NND in dual labeled cells reveals two populations between spectrin βII clusters (**E**) and one for spectrin βII-Cav1.3 (**F**). (**G-J**) NNMF analysis defines a periodic pattern for cluster rows (**G** and **H**) or a single distribution for isolated clusters (**I** and **J**). Sample values (n) = cells, θ = features. R^2 value in (**E**) corresponds to the superimposed combined fit for the two populations. Scale bars: (**A** and **C**) 5 µm; (**B,** ROI-1, -2; **D,** ROI-1), 2 µm; (**D,** ROI-2), 500 nm. Bin widths: (**E-F**) 25 nm, (**G-H**) 15 nm, (**I-J**) 20 nm. See also ***Supplemental Table 1 and 2.***

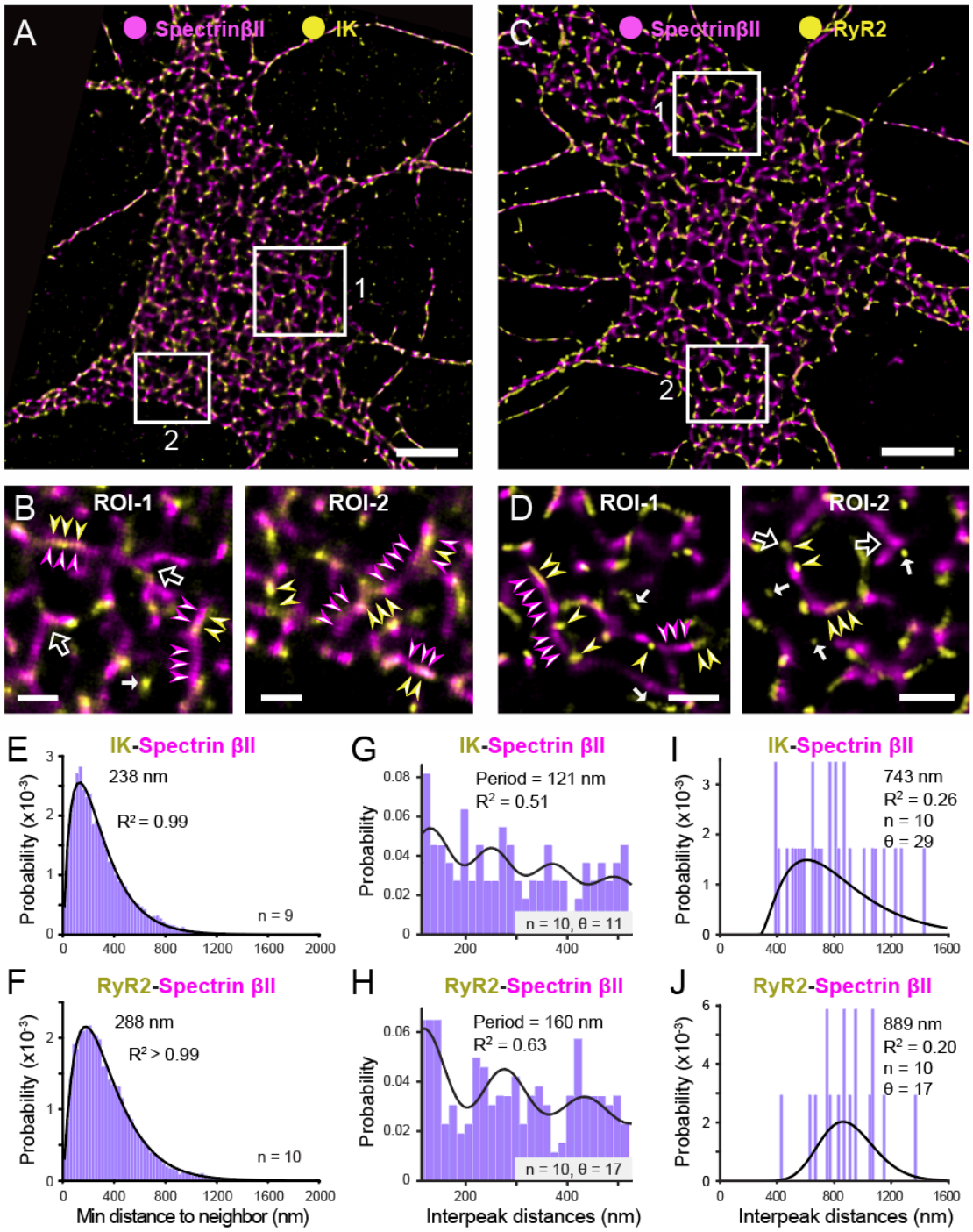

Figure 4. Spectrin exhibits an organized pattern that is closely associated with IK and RyR2 distributions. (**A-D**) STORM-TIRF images of immunolabeled clusters for the indicated proteins. Larger field views (**A** and **C**) with ROIs magnified (**B** and **D**) identify rows of spectrin βII clusters that can reach branch points (*open arrows*) that colocalize or alternate with rows of IK or RyR2 (*arrowheads*). Isolated clusters can be distinguished for IK or RyR2 (**B,** ROI-2, **D**, ROI-1, 2; *filled arrows*). (**E-F**) NND analysis between IK-spectrin βII (**E**) and RyR2-spectrin βII (**F**). (**G-J**), NNMF analysis defines a periodic pattern for cluster rows (**G-H**) or a single distribution for isolated clusters (**I-J**). Sample values (n) = cells, θ = features. Scale bars: (**A** and **C**) 5 µm; (**B** and **D**, ROI-1, -2), 1 µm. Bin widths: (**E-F**) 25 nm, (**G-H**) 15 nm, (**I-J**) 20 nm. See also ***Supplemental Figure 3, Supplemental Table 1 and 2***.

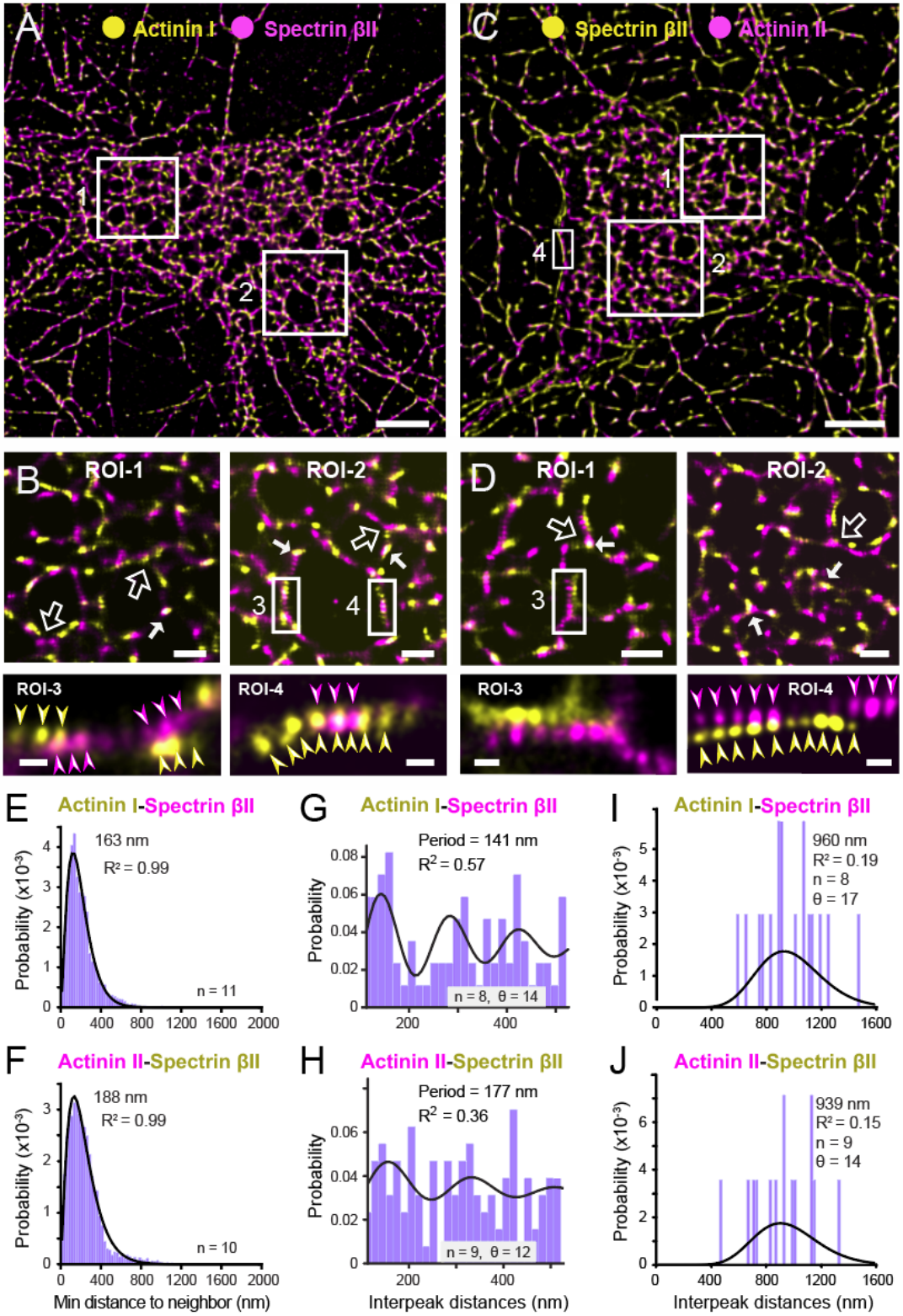

Figure 5. Actinin I and actinin II exhibit an organized pattern in relation to spectrin βII. (**A-D**) STORM-TIRF images of immunolabeled clusters for the indicated proteins. Shown are dual labeled images for spectrin with actinin I (**A-B**) or with actinin II (**C-D**), with ROIs magnified in (**B** and **D**). Rows of spectrin βII or actinin clusters can extend to branch points (*open arrows*), colocalize (*solid arrows*), or alternate to extend or bridge rows of labels (*arrowheads*).

(**E-F**) NND analysis between actinin I-spectrin βII (**E**) and actinin II-spectrin βII (**F**).

(**G-J**) NNMF analysis defines a periodic pattern for cluster rows (**G-H**) or a single distribution for isolated clusters (**I-J**). Sample values (n) = cells, θ = features. Scale bars: (**A** and **C**) 5 µm; (**B** and **D,** ROI-1, 2), 1 µm; (**B** and **D,** lower ROIs), 200 nm. Bin widths: (**E-F**) 25 nm, (**G-H**) 15 nm, (**I-J**) 20 nm. See also ***Supplemental Figure 4, Supplemental Table 1 and 2.***

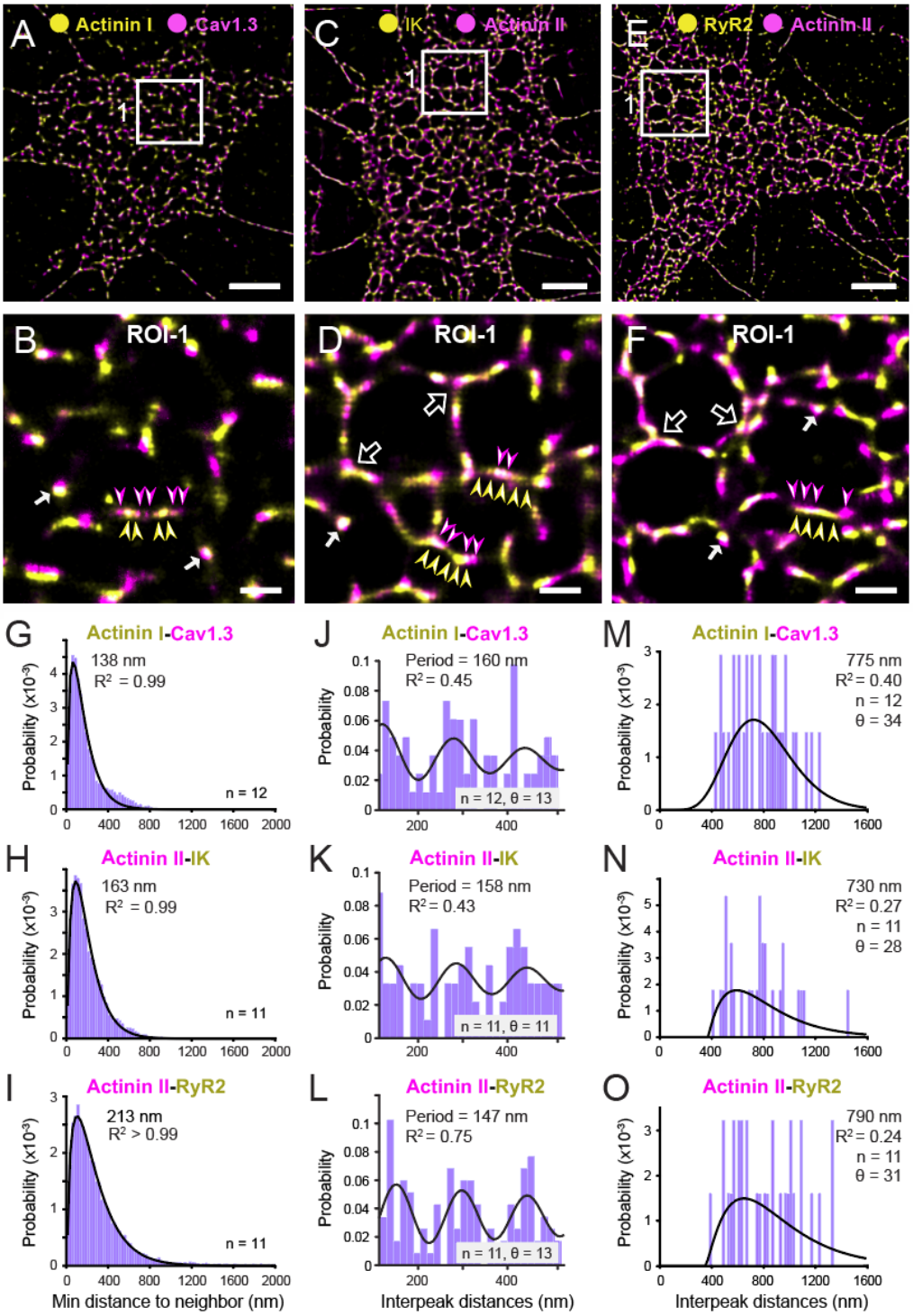

Figure 6. Actinin I and actinin II distributions are aligned with CaRyK complex proteins. (**A-F**) STORM-TIRF images of immunolabeled clusters for the indicated proteins. Shown are dual labeled images for the indicated CaRyK complex proteins and actinin isoforms. Larger field views (**A, C, E**) and associated ROIs (**B, D, F**) identify clusters that align in rows that either overlap or alternate (*arrowheads*) with actinin isoforms. Cluster rows can extend to branch points (*open arrows*), colocalize (*solid arrows*), or alternate to extend or bridge rows of labels (*arrowheads*). (**G-I**) NND analysis between actinin I - Cav1.3 (**G**), actinin II - IK (**H**) and actinin II - RyR2 (**I**). (**J-O**) NNMF analysis defines a periodic pattern for cluster rows (**J-L**) or a single distribution for isolated clusters (**M-O**). Sample values (n) = cells, θ = features. Scale bars: (**A, C, E**) 5 µm; (**B, D, F**), 1 µm. Bin widths: (**G-I**) 25 nm, (**J-L**) 15 nm, (**M-O**) 20 nm. See also ***Supplemental Table 1 and 2.***

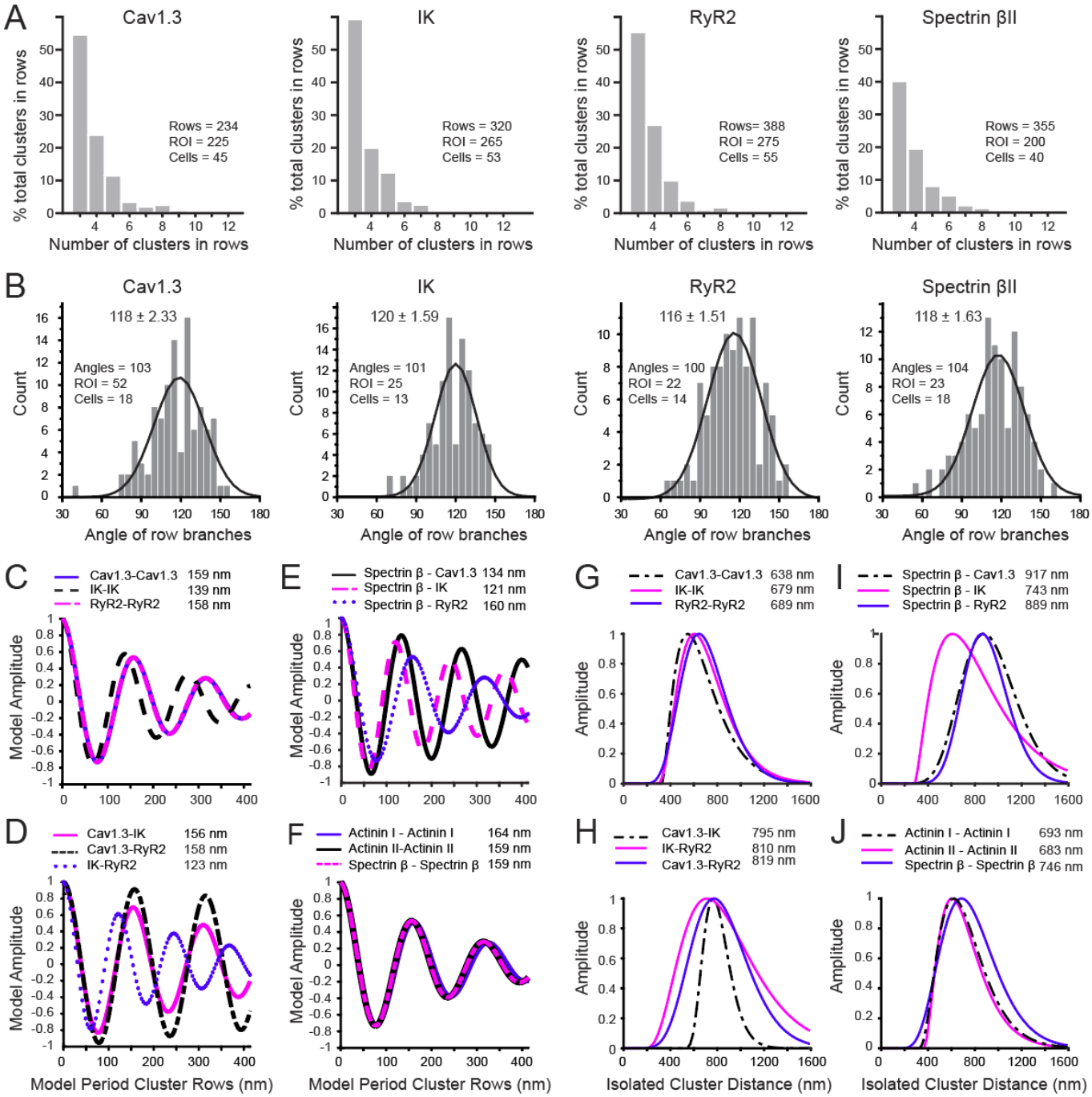

Figure 7. Correspondence between the spatial organization of CaRyK complex proteins and spectrin. (**A**) Plots of the percent of clusters aligned in rows of at least three clusters for the indicated immunolabels. (**B**) Plots of the angles at branch points of cluster rows for the indicated immunolabels. Bin widths: 5 degrees. (**C-J**) Comparison of model fits for cluster rows (**C-F**) and fits for isolated clusters (**G-J**) for the indicated pairs of immunolabels. The damped oscillatory models are amplitude and phase shift normalized for comparison (first crest of fit, 0 nm) (**C-F**) and gamma model centers are amplitude normalized (**G-J**). Gaussian fits are used for plots in (**B**) and average values are mean ± SEM. Fits in (**C-E**) are from ***Supplemental Figure 1-4, Supplemental Table 1-4.***

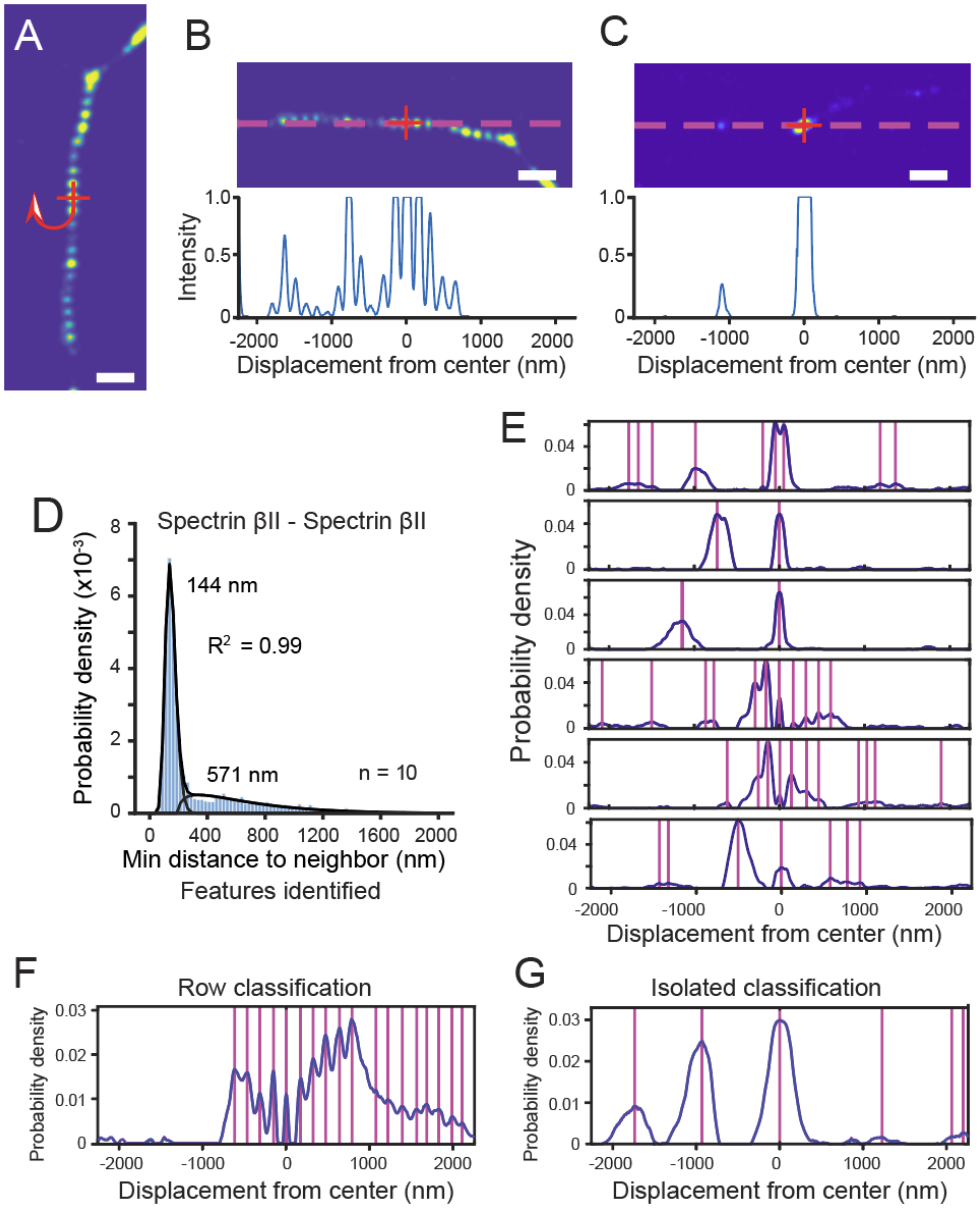

Figure 8. The use of NNMF to define patterns in immunolabeled cluster centroids. (**A-C**) Procedure to define relationships between immunolabeled clusters in representative STORM-TIRF images of neuronal processes outside of the soma labeled for spectrin βII. A systematic pixel-by-pixel search identifies the center of a detected centroid (**A,** *cross*) for spectrin βII labeling. Images are then rotated to a position where its nearest neighboring centroid is oriented to the left and the ROI is stored for feature detection (**B-C**). Below the images in (**B-C**) are 1D displays of normalized pixel intensity aligned with the profile indicated by *dashed lines* for a row of clusters consistent with the MPS (**A-B**) as well as isolated clusters (**C**). (**D**) NND analysis of spectrin βII clusters in neuronal processes reveal two populations of inter cluster distances, with the majority fitting a distribution with a median value of 144 nm. (**E**) Representative example of centroid features extracted by NNMF from spectrin βII labeled neural processes outside the soma of a single cell with k = 6. *Vertical lines* denote detected peak positions. (**F-G**) Two representative examples of features containing rows (**F**) or isolated clusters (**G**) for spectrin βII labeling. Scale bars: (**A-C**) 500 nm. Bin width (**D**) 25 nm.

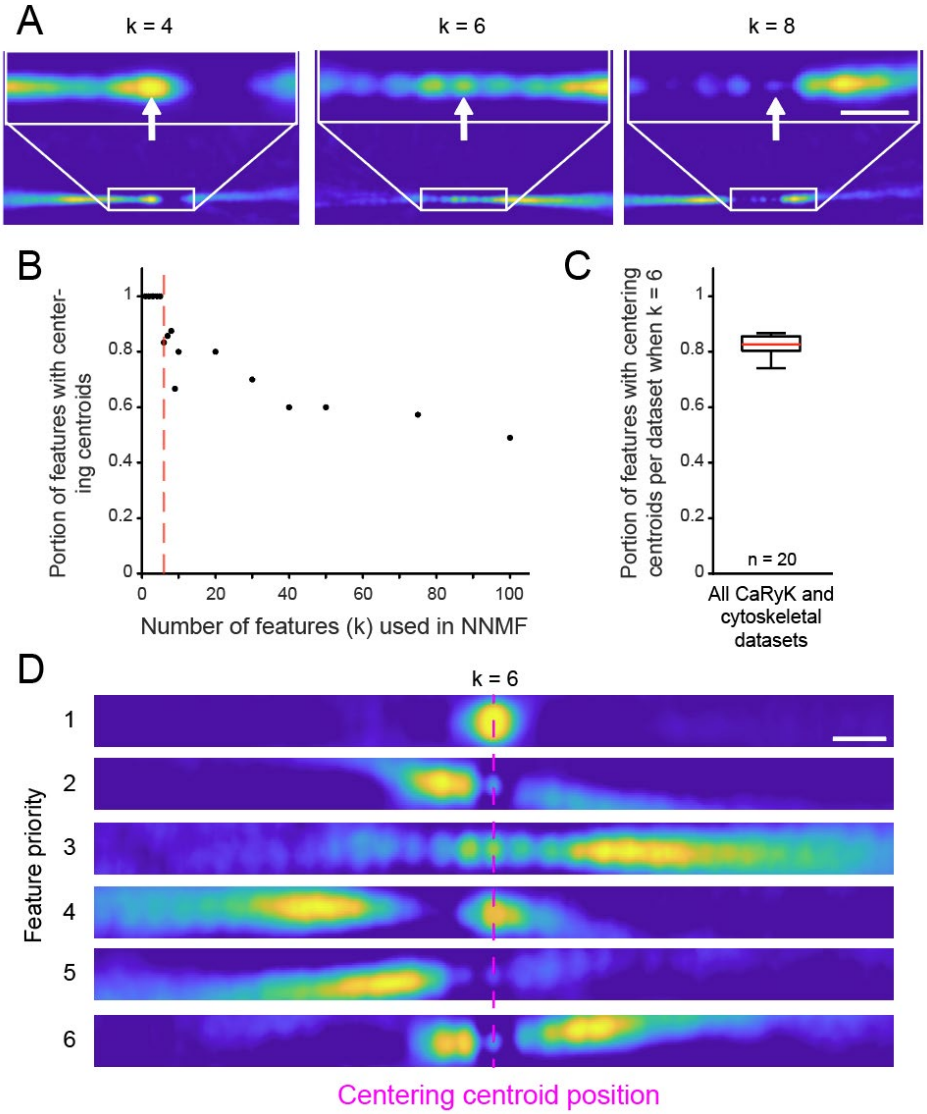

Figure 9: Rationale for feature number selection for NNMF. The effects of using different numbers of features (k) to calculate the distance between rows of clusters using NNMF. NNMF generates features as rows of a matrix which are reported in decreasing importance to the original data set. Every cluster centroid image prior to input into NNMF has a central point spread function upon which the image is aligned to identify intercluster distances of neighboring rows of clusters. (**A**) A representative case of feature detection for different k values for spectrin βII images, with each case illustrating the third feature calculated by NNMF. ROIs of the regions indicated by a *white box* are shown expanded above. As k increases, attributes of each feature become diluted until the central centroid (*white* arrows) becomes diminished or is no more prominent than noise (i.e. k = 8). (**B**) Scatter plot showing a progressive loss of central centroids in downstream analysis as the number of features generated is increased. *Red dashed line* indicates k = 6 (portion = 0.8333). (**C**) Box plot of the portion of features across CaRyK, spectrin and actinin datasets which contain a detectable central centroid to calculate intercluster distances in rows of immunolabeled clusters (mean = 0.824 ± 0.0075). Analyses were conducted with k = 6 to avoid instances where the centering centroid was miniscule or absent and ensure that features reflected a plausible centroid image while maximizing the number of features for downstream analysis. (**D**) Representative example of the top six features extracted for spectrin βII in MAP2 positive or negative processes of hippocampal cells. Scale bars: (**A**, ROIs) 300 nm, (**D**) 300 nm. Sample values (n) in (**C**) reflect all data sets for CaRyK, spectrin and actinin immunolabels.

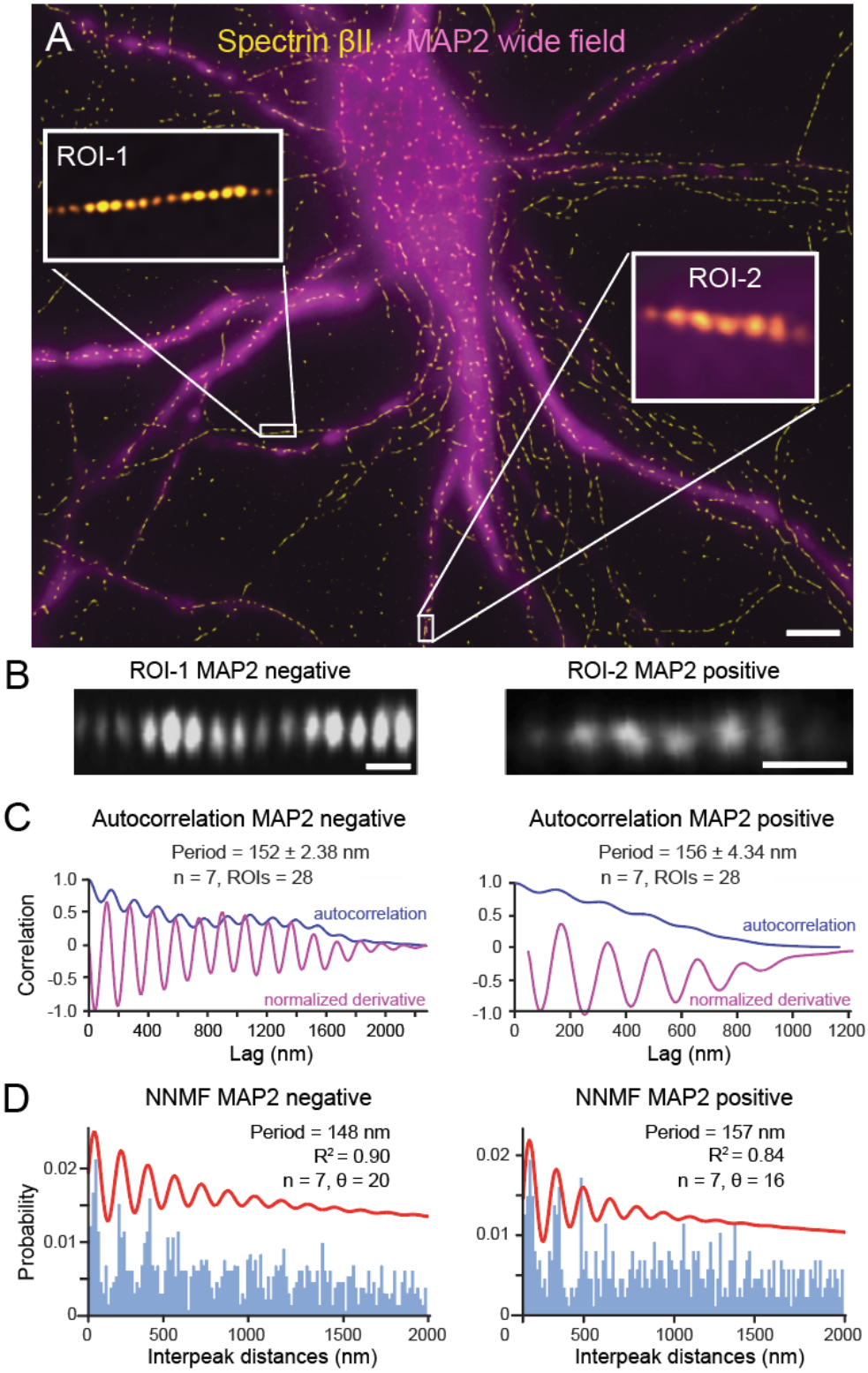

Figure 10. Comparison of periodicity in cluster organization measured by autocorrelation vs NNMF. (**A-B**) Representative STORM-TIRF image of spectrin βII labeling with an overlaid larger field image of MAP2-GFP labeling (**A**). Two processes are highlighted as MAP2 negative putative axons (ROI-1) and MAP2 positive putative dendrites (ROI-2) (**B**). (**C-D**) Spectrin βII labeling of MAP2 negative or MAP2 positive processes outside of the soma are analyzed for periodicity by autocorrelation (**C**) or NNMF (**D**). In (**C**) the autocorrelations (*blue lines*) and normalized derivatives (*magenta lines*) are shown superimposed and drawn from the specific ROI examples in (**B**), while mean periods are calculated from the entire population of clusters. In (**D**) histograms of interpeak distance of row classified spectrin βII features from the same data set are shown superimposed with the damped oscillatory model fits (*red lines*) calculated by NNMF. Scale bars: (**A**) 5 µm, (**A**, inset ROI-1,2) 500 nm, (**B,** ROI-1, 2) 300 nm. Average values are mean ± SEM. Sample values (n) = cells, θ = NNMF row features (**E**). Bin widths: (**D**) 15.4 nm.

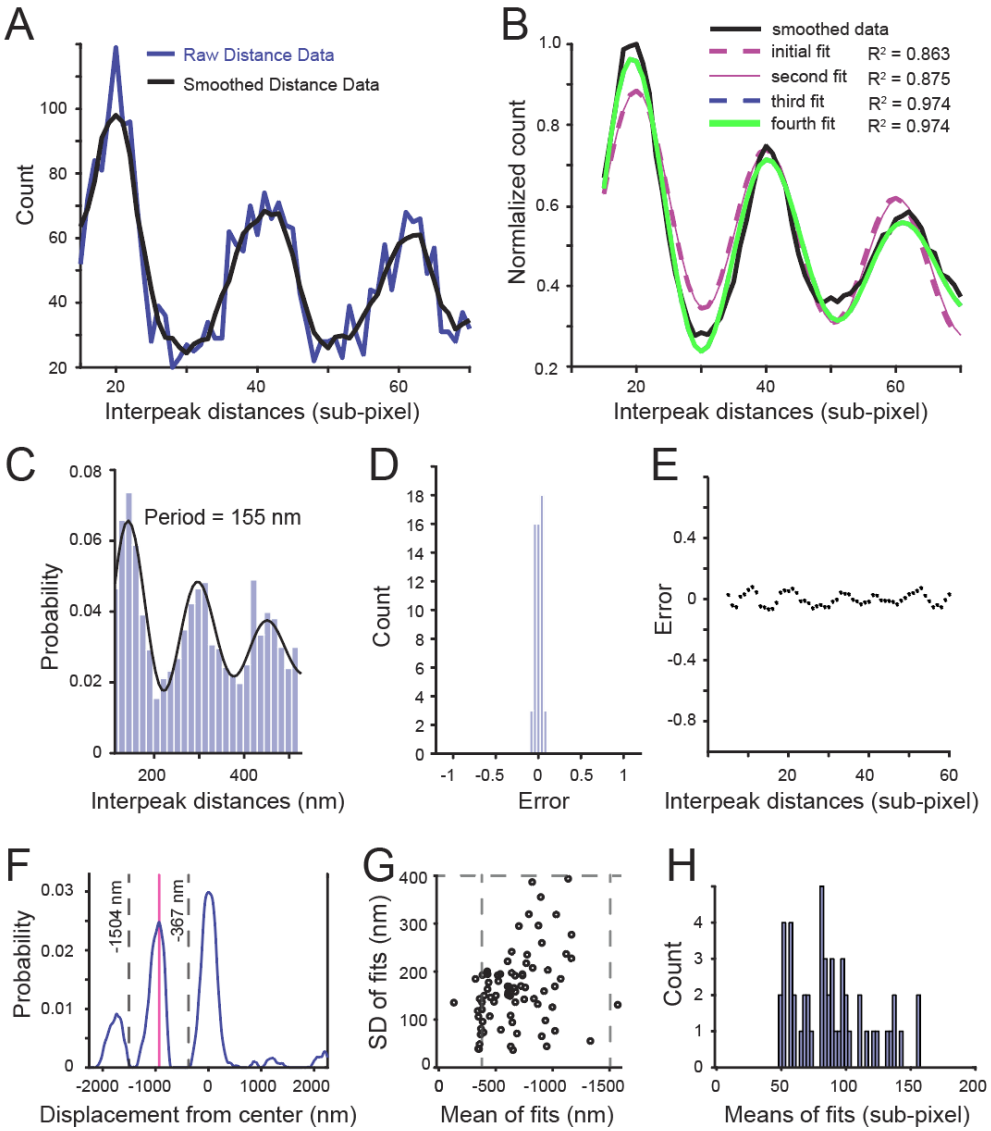

Figure 11. Defining inter cluster distances from NNMF. Procedure for oscillatory model fitting of the NNMF defined interpeak distance histograms. (**A**) Plot of the heights of binned interpeak distances of the initial 3 cycles of row classified features generated by NNMF of spectrin βII labeled processes. Interpeak distances are cropped to a range of 15-70 sub-pixels to accommodate the highest S/N region. Shown superimposed is data before and after smoothing with a moving average to improve model fit. (**B**) Superimposed records of smoothed data trace from (**A**) fit with a damped oscillatory model for 4 iterations using a least-squares method. (**C-E**) Representative example of best fit model and error values for spectrin βII NNMF calculations in processes, with the best fit model (*black line*) superimposed on the histogram of raw interpeak distance data in (**C**). Shown in (**D-E**) is the histogram of error between model and data (**D**), with error distributed around zero. A scatter plot of error along the X axis of data in (**C**) is relatively homoscedastic (**E**). (**F-H**) Procedure for defining peak centers of isolated features identified by NNMF. A representative example of an isolated classified feature as a plot of probability in relation to distance from centering centroid for spectrin βII - spectrin βII (**F**). An examination window of -1504 to -367 nm (*gray dashed lines*) is used to avoid the influence of the centering centroid or distant data tails in defining the peak of isolated clusters (*magenta vertical line*) (**F**). (**G**) Data within the examination window is fit with a single gaussian. A plot of the mean and SD of fits of isolated cluster gaussians is used to confirm a single population of gaussians and eliminate outliers defined using *rmoutliers*. Any gaussians that fell outside of the examination window (*gray dashed lines*) were removed, along with gaussians that were not well fit to the data they represented ($R^2 \leq 0.9$). (**H**) Final histogram of accepted means for isolated cluster distances determined in (**F-G**). Bin widths: (**C**) 15 nm, (**D**) 0.04, (**H**) 20 nm.

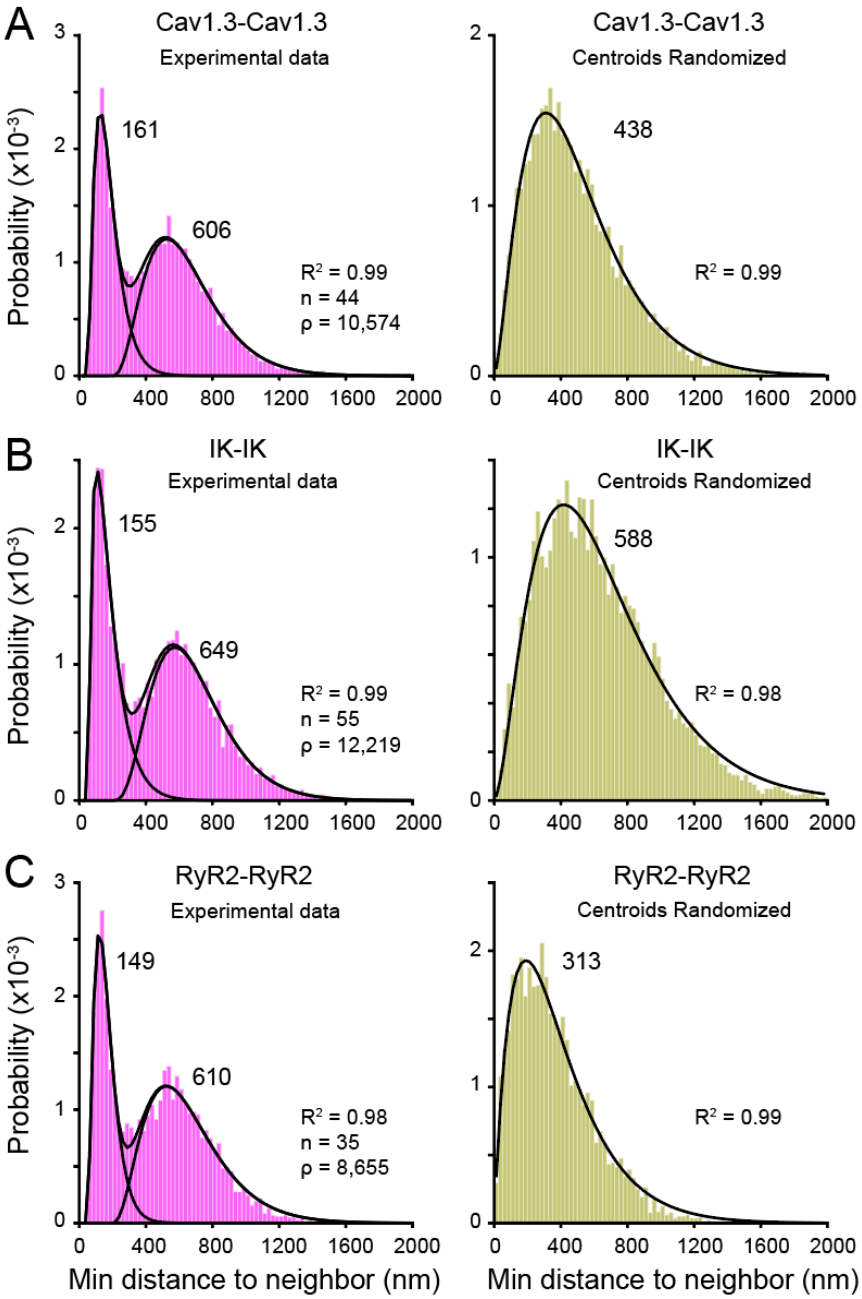

Supplemental Figure 1. The spatial distribution of CaRyK complex immunolabeled clusters at the soma is not random. Related to ***Figure 1 and 2***. (**A-C**) *Left column* provides NND distributions of the indicated CaRyK complex proteins. *Right column* indicates NND distributions for the same datasets after randomizing centroid positions. Significant differences exist between experimental and randomized data for each protein (non-parametric 2- sample Kolmogorov–Smirnov test (KS)): (**A**) $p < 0.001$, KS-stat = 0.1180; (**B**) $p < 0.001$, KS-stat = 0.1999; (**C**) $p < 0.001$, KS-stat = 0.1957). Numerical indicators adjacent to histograms represent median values. Sample values (n) = cells, ρ, number of centroids detected across all images for a given label set. Bin widths: (**A-C**) 25 nm.

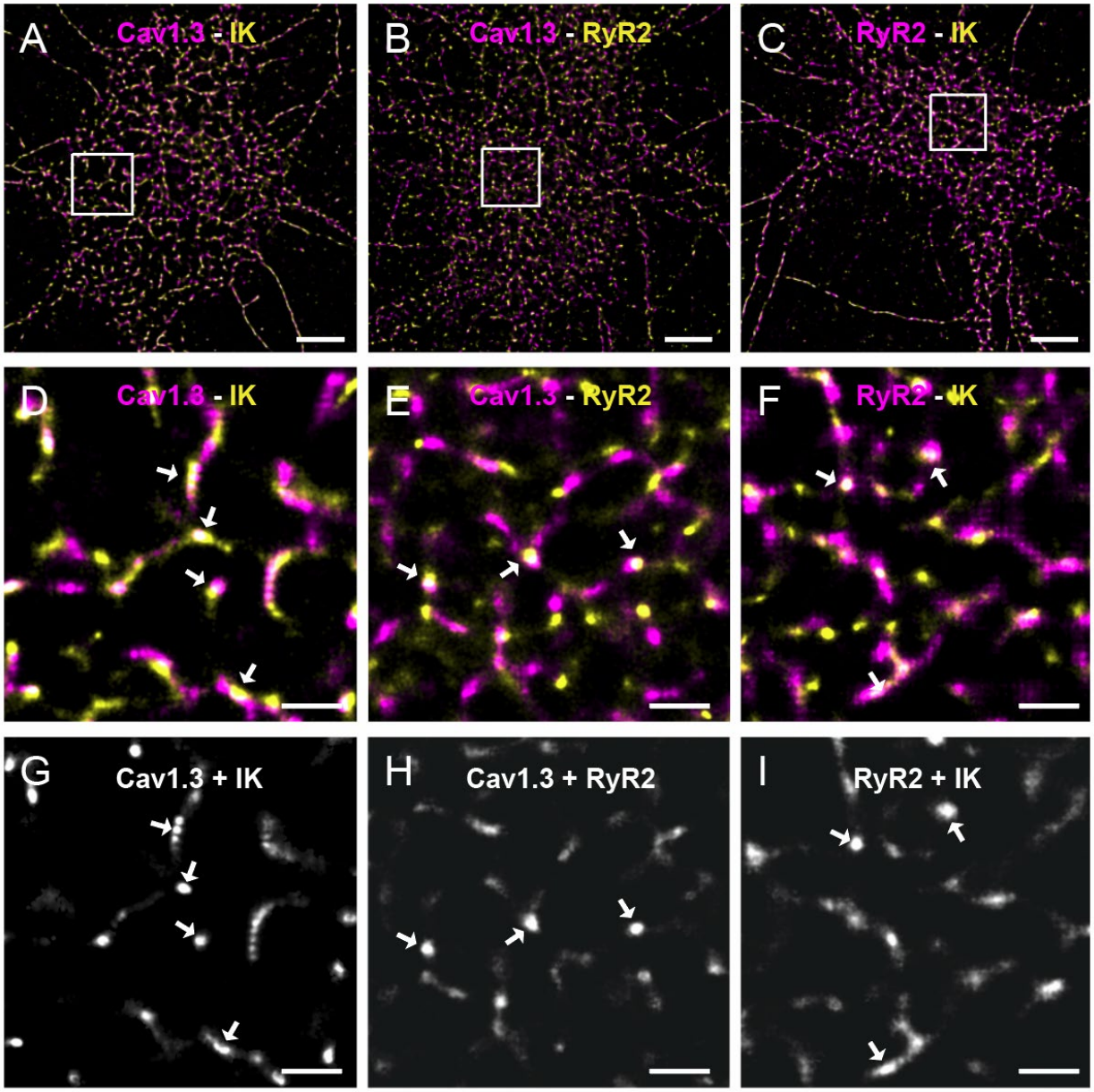

Supplemental Figure 2. Related to *Figure 1 and 2.* Generating images of fluorescent emission overlap for NNMF analysis. Related to Figures 1-6. (**A-C**) Larger field views of hippocampal neurons dual immunolabeled for the indicated proteins. (**D-F**) Expanded views of ROIs from images in (**A-C**) illustrating overlap of some fluorescence emissions (white chroma, *arrows*) suggestive of protein colocalizations. (**G-I**) Black and white images of overlap-dependent intensity representations of the dual labels in (**D-F)** to apply NNMF on dual labeled clusters. Pixel intensity of the overlap image is determined pixel wise by:

$$Overlap_{xy} = \sqrt{(Green\ Intensity_{xy})(Red\ Intensity_{xy})}.$$

Scale bars: (**A-C**) 5 µm; (**D-I**), 500 nm. See also ***Supplemental Table 4.***

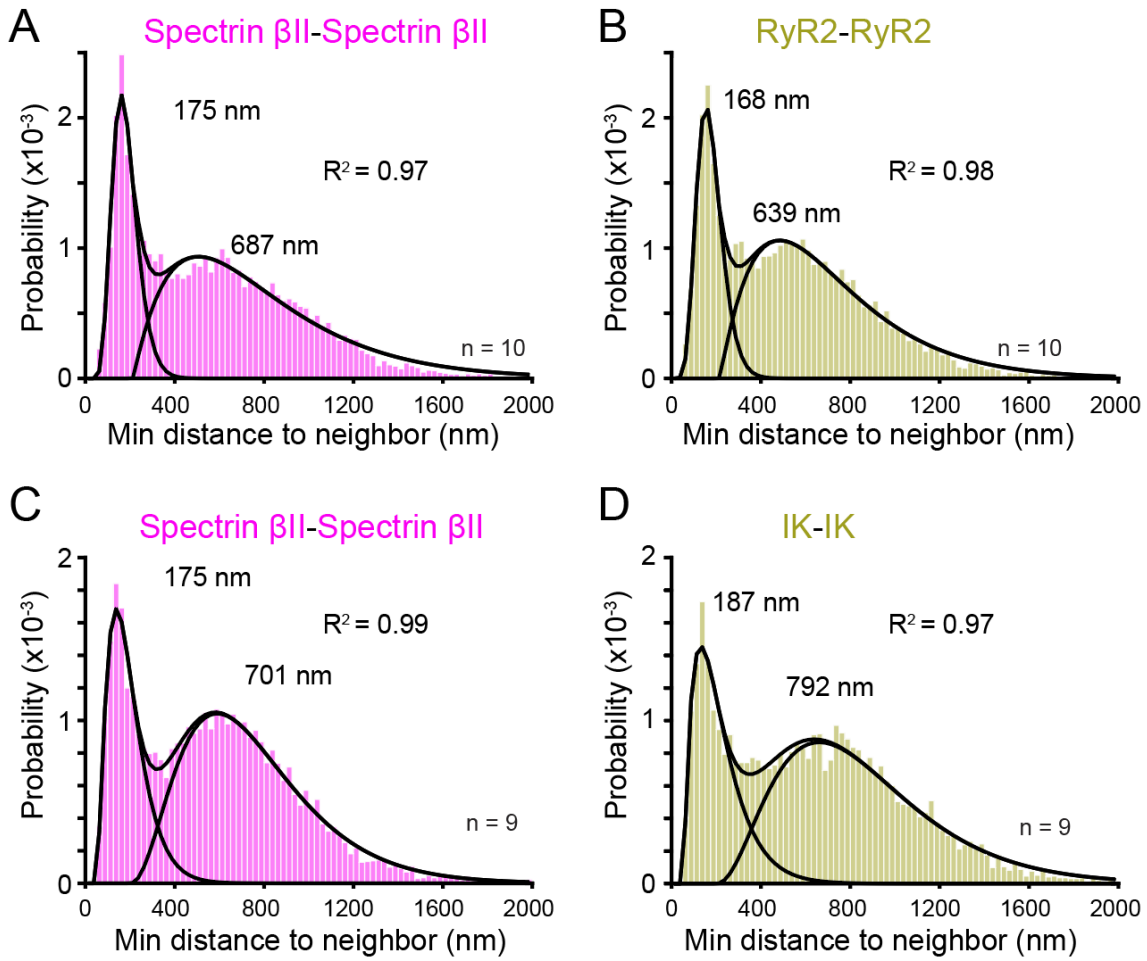

Supplemental Figure 3. Spectrin βII clusters distribute with similar patterns as IK and RyR2. ***Related to Figure 3 and 4.*** (**A-D**) NND histograms of similar immunolabels in two sets of dual labeled tissue (**A-B,** spectrin βII-RyR2; **C-D,** spectrin βII-IK) reveals populations that can be described by two gamma fits. Values are the median of fit gamma distributions and R^2 of the combined fits. Sample values (n) represent the number of individual cells analyzed. Bin widths: 25 nm.

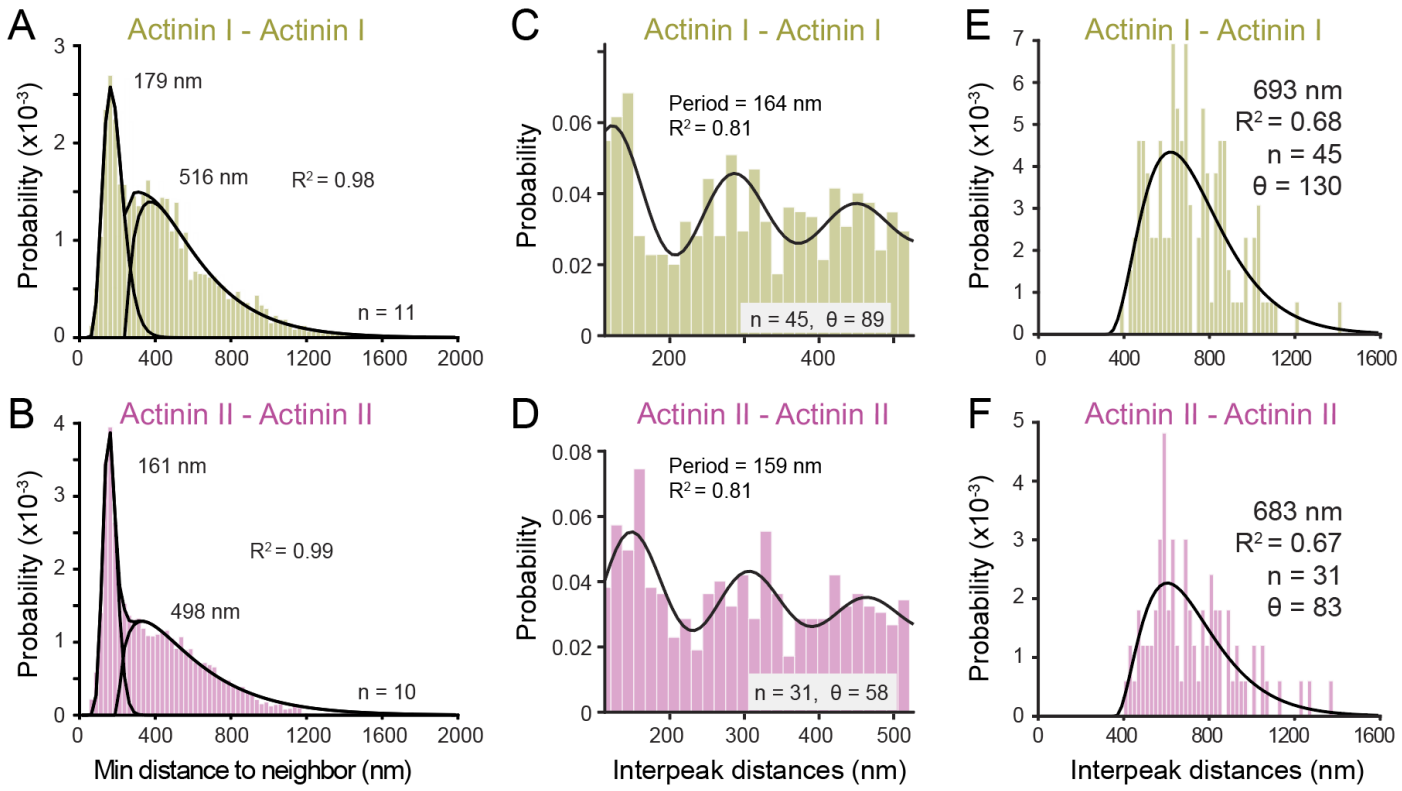

Supplemental Figure 4. Actinin I and actinin II immunolabels exhibit a structured pattern indicative of rows and isolated clusters. Related to *Figure 5.* (**A-B**) NND analysis within actinin I clusters (**A**) and actinin II clusters (**B**) reveal two populations of inter-centroid distance fit with two gamma distributions. Distributions are comparable to that of spectrin βII (see **Figs. 3 and S7**). (**C-F**) NNMF analysis of the indicated immunolabels defines a regular periodicity of cluster rows (**C-D**) or isolated clusters (**E-F**). Medians of gamma distributions, R^2 values of fitted gamma distributions (**A, B, E,** and **F**), model periods and with their associated R^2 values (**C-D**) are indicated on plots. Total number of centroids detected to apply NNMF (**C-F**): actinin I-actinin I, 19,767; actinin II-actinin II, 21,634. Sample values (n)= cells, θ = features. Bin widths: (**A-B)** 25 nm, (**C-D**) 15 nm, (**E-F**) 20 nm.

Dual Labeled Tissue	Cluster Pairs	n	First Median (nm)	Second Median (nm)	R^2	Mixing % of first gamma in GMM
Cav1.3 - IK	Cav1.3 -Cav1.3	11	169	664	0.9773	27.2
	IK-IK		177	699	0.9827	27.7
	Cav1.3-IK		188	-	0.9935	100
IK - RyR2	IK - IK	11	186	722	0.9822	28.1
	RyR2 - RyR2		169	635	0.9888	33.2
	IK - RyR2		238	-	0.9973	100
Cav1.3 - RyR2	Cav1.3 - Cav1.3	9	174	624	0.9904	34.8
	RyR2 - RyR2		185	755	0.9822	25.1
	Cav1.3 - RyR2		238	-	0.9978	100
Cav1.3 - Spectrin βII	Cav1.3 - Cav1.3	13	168	649	0.9854	30.3
	Spectrin βII - Spectrin βII		183	733	0.9783	26.8
	Cav1.3 - Spectrin βII		288	-	0.9955	100
IK - Spectrin βII	IK - IK	9	187	792	0.9718	31.8
	Spectrin βII - Spectrin βII		175	701	0.9879	31.1
	IK - Spectrin βII		238	-	0.9939	100
RyR2 - Spectrin βII	RyR2 - RyR2	10	168	639	0.9854	28.9
	Spectrin βII - Spectrin βII		175	687	0.9720	29.4
	RyR2 - Spectrin βII		288	-	0.9959	100
Cav1.3 - Actinin I	Cav1.3 - Cav1.3	12	180	641	0.9902	23.2
	Actinin I- Actinin I		192	667	0.9870	18.2

	Cav1.3 - Actinin I		138	-	0.9880	100
IK - Actinin I	IK - IK	11	164	729	0.9872	27.7
	Actinin I - Actinin I		174	683	0.9757	27.6
	IK - Actinin I		363	-	0.9945	100
RyR2 - Actinin I	RyR2 - RyR2	10	168	704	0.9773	
	Actinin I - Actinin I		179	718	0.9790	
	RyR2 - Actinin I		338	-	0.9931	
Spectrin βII - Actinin I	SpectrinβII - SpectrinβII	9	170	489	0.9812	
	Actinin I - Actinin I		179	516	0.9780	
	SpectrinβII - Actinin I		163	-	0.9859	100
IK- Actinin II	IK- IK	11	218	726	0.9800	42.5
	Actinin II- Actinin II		169	611	0.9901	34.2
	IK- Actinin II		163	-	0.9922	100
RyR2- Actinin II	RyR2- RyR2	10	186	730	0.9799	24.9
	Actinin II - Actinin II		166	628	0.9822	29.1
	RyR2- Actinin II		213	-	0.9966	100
Spectrin βII - Actinin II	SpectrinβII - SpectrinβII	10	161	498	0.9903	35.0
	Actinin II - Actinin II		161	452	0.9807	34.9
	SpectrinβII - Actinin II		188	-	0.9886	100

Supplemental Table 1. Summary comparisons of fitted gamma mixture models on NND for the indicated protein pairs. All cells were imaged with two immunolabel targets and nearest neighbor distance (NND) distributions calculated for all clusters. NND was calculated using LAMA's morphological cluster analysis and fitted with a mixed gamma model to define central tendency for each gamma distribution in the NND histograms of ***Figure 1-6.*** Cluster pairs = the labeled targets which are being compared to generate the NND histogram. n = the number of cells. R^2 = coefficient of determination when comparing the sum of fitted gamma distributions to the NND histogram. GMM = gamma-mixture model.

				Row Cluster Data			Isolated Cluster Data	
Dataset	**n**	**Centroids x10^3**	**θ**	**Period (nm)**	**R^2**	**SSQ**	**Median (nm)**	**R^2**
Cav1.3 - Cav1.3	45	36.8	270	159	0.846	0.221	638	0.733
IK - IK	53	32.7	318	139	0.873	0.127	714	0.653
RyR2 - RyR2	55	43.1	330	158	0.861	0.172	711	0.543
Spectrin βII - Spectrin βII	50	34.4	300	159	0.920	0.121	774	0.558
Actinin I - Actinin I	45	19.8	270	164	0.810	0.230	693	0.681
Actinin II - Actinin II	31	21.6	186	159	0.813	0.225	683	0.674
Cav1.3 - IK	11	4.1	66	156	0.647	0.612	795	0.308
Cav1.3 - RyR2	9	3.1	54	158	0.484	0.999	819	0.165
RyR2 - IK	11	4.4	66	123	0.724	0.497	810	0.170
Cav1.3 - Spectrin βII	13	5.6	78	134	0.625	0.404	917	0.165
RyR2 - Spectrin βII	10	3.3	60	160	0.626	0.508	889	0.203
Spectrin βII - IK	10	6.4	60	121	0.509	0.710	743	0.263
Cav1.3 - Actinin I	12	4.2	72	160	0.453	1.053	775	0.396
IK - Actinin I	11	3.5	66	171	0.529	0.791	906	0.141
RyR2 - Actinin I	14	3.1	84	159	0.743	0.447	868	0.382
Spectrin βII - Actinin I	8	6.3	48	141	0.574	0.983	960	0.192
Actinin II - IK	11	7.9	66	158	0.431	0.931	730	0.227
Actinin II -RyR2	11	4.1	66	147	0.754	0.740	790	0.238
Actinin II -Spectrin βII	9	4.7	54	177	0.356	1.027	939	0.154

Supplemental Table 2. Summary of NNMF feature analysis for the indicated protein pairs. Information about data entered into the NNMF workflow and the results. n = the number of cells imaged. Centroids = the sum of weighted positions across all images that were assessed by NNMF to generate features. Θ = the number of features generated per label set. Row Cluster Data = features from NNMF which were assessed for peak density anticipated in regular and repeating clusters. Isolated Cluster Data = features from NNMF which were assessed with a low peak density anticipated by isolated centroids. Period = period of fitted damped oscillatory model on interpeak data from features. R^2 = coefficient of determination when comparing data to the fitted model. SSQ = sum of squared error between smoothed interpeak data and the

fitted model. Median center = displacement of fitted gamma on isolated features from their reference position. Empty cells represent instances where no interpretable data was produced.

	Welch 2 sample T-test			KS-test	
Angle comparisons	**t-stat**	**df**	**p-value**	**k-stat**	**p-value**
Cav1.3 - IK	-0.5008	197.16	0.6171	0.0925	0.7758
Cav1.3 - RyR2	0.2621	201	0.7935	0.0884	0.8232
IK - RyR2	0.7878	194.07	0.4318	0.1224	0.4392
Spectrin βII - Cav1.3	0.5033	208.84	0.6153	0.0813	0.8836
Spectrin βII - IK	1.0333	196.39	0.3027	0.1219	0.4321
Spectrin βII - RyR2	0.2486	201.87	0.8039	0.0577	0.9958
Spectrin βII - Actinin I	-1.378	214.27	0.1697	0.1141	0.4628
Spectrin βII - Actinin II	-0.2847	105.57	0.7764	0.0962	0.8982
Actinin I - Cav1.3	-0.8699	215.32	0.3853	0.0924	0.7313
Actinin I - IK	-0.4210	219	0.6742	0.0947	0.7088
Actinin I - RyR2	-1.149	212.22	0.2519	0.1133	0.4852
Actinin II - Cav1.3	0.1312	102.41	0.8959	0.0812	0.9571
Actinin II - IK	0.5372	88.523	0.5924	0.0851	0.9648
Actinin II - RyR2	-0.0825	100.95	0.9344	0.1115	0.7387

Supplemental Table 3. The distribution of cluster row branchpoint angles are not significantly different. With sample size > 100 normality assumption was ignored and Welch 2 sample t-test was used to compare the central tendency of distributions. Two sample Kolmogorov-smirnov (KS) test was used to test the null hypothesis of the distributions being from the same population. Statistical calculations were completed using R software. df, degrees of freedom. See also ***Figure 7B***.

Red Label	Green Label	n	% Overlap on Red	% Overlap on Green
Cav1.3	IK	11	22.5 ± 1.5	20.4 ± 1.9
RyR2	IK	11	13.0 ± 1.8	18.2 ± 1.7
Cav1.3	RyR2	9	9.6 ± 1.1	16.2 ± 1.6

Supplemental Table 4. Percent overlap of pixels labeled for CaRyK complex proteins. Dual labeled images were masked to their ROIs, thresholded at > 20% maximal intensity and all pixels were counted. When pixels in the same position in both channels were greater than the threshold, they were counted as overlapped and divided by the sum of pixels greater than threshold in each channel. Calculated in MATLAB with custom scripts.

REAGENT	SOURCE	IDENTIFIER
Antibodies		
Rabbit polyclonal anti-Cav1.3 (1:250)	Alomone Labs	ACC-005; RRID:AB_2039775
Mouse monoclonal anti-Cav1.3 (1:250)	Novus Biologicals	NBP2-12893
Mouse monoclonal anti-KCa3.1 (1:250)	Santa Cruz Biotechnology	sc-365265; RRID:AB_10841432
Mouse monoclonal anti-RyR2 (C3-33) (1:200)	Sigma-Aldrich	R-128; RRID:AB_261301
Rabbit polyclonal anti-RyR2 (1:200)	Sigma-Aldrich	SAB4502707; RRID:AB_10746831
Rabbit polyclonal anti-BII-Spectrin (1:250)	Abcam	ab72239; RRID:AB_1270902
Mouse monoclonal anti-BII-Spectrin (1:250)	BD Transduction	612563; RRID:AB_399854
Goat anti-Actinin-I (1:250)	Novus Biologicals	AF8279;
Rabbit monoclonal anti-Actinin-II (1:250)	Abcam	ab68167; RRID:AB_11157538
Chicken polyclonal anti-microtubule-associated protein (MAP2) (1:500)	Abcam	ab5932; RRID:AB_92147
Goat F(ab´)$_2$ anti-rabbit IgG – Alexa Flour-647 (1:1000)	Jackson ImmunoResearch	111-606-047; RRID:AB_2338082
Rabbit F(ab´)$_2$ anti-mouse IgG – Cy3 (1:1000)	Jackson ImmunoResearch	315-166-047; RRID:AB_2340148
Rabbit F(ab´)$_2$ anti-chicken IgG – Alexa Fluor-488 (1:1000)	Jackson ImmunoResearch	303-546-003; RRID:AB_2339330
Donkey F(ab') anti-rabbit IgG – Alexa Fluor-647 (1:1000)	Jackson ImmunoResearch	711-606-152; RRID:AB_2340625
Goat F(ab') anti-mouse IgG – Cy3 (1:1000)	Jackson ImmunoResearch	115-166-146; RRID:AB_2338708
Donkey F(ab') anti-goat IgG – Cy3 (1:1000)	Jackson ImmunoResearch	705-166-147; RRID:AB_2340413
Chemicals, peptides, and recombinant proteins		
Isoflurane	Fresenius Kabi	Cat No. CP0406V2
Papain	Worthington	Cat No. LS003126
Dubecco's PBS	Sigma Aldrich	Cat No. D8537-500ML
Bovine Serum Albumin	Vector Laboratories	Cat No. SP-5050
Normal Goat Serum	Jackson ImmunoResearch	Cat No. 005-000-121
Glucose oxidase (Aspergellius Niger)	Sigma Aldrich	Cat No. G2133-50KU
Catalase (Bovine)	Sigma Aldrich	Cat No. C3155-50MG
Beta-Mercaptoethanol	Sigma Aldrich	Cat No. M6250-100ML
Triton-X	Sigma Aldrich	Cat No. T-8787
Poly-L-Lysine	Sigma Aldrich	Cat No. P-7280
Neurobasal Medium	Invitrogen	Cat No. 21010-046
Pyruvate	Invitrogen	Cat No. 11360-070
Glutamine	Invitrogen	Cat No. 25030-081
B-27	Invitrogen	Cat No. 17504-044
Pen-Streptomycin	Invitrogen	Cat No. 15140-122
Laminin	Sigma Aldrich	Cat No. L2020
FBS	Gibco	Cat No. 26140-079
HEPES	Sigma Aldrich	Cat No. H3375
Glucose	Sigma Aldrich	Cat No. G8270

TetraSpek™ beads (100 nm diameter)	Thermo Fisher Scientific	Cat No. T7279
MACS BSA solution	Miltenyi Biotec	Cat No. 130-091-376
Microglia microbeads	Miltenyi Biotec	Cat No. 130-105-634
Other		
No. 1.5 18 mm Coverslip	Electron Microscopy Sciences	Cat No. 72222-01
70 µm separation filter	Corning	Cat No. 07201431
Minimacs Separator	Miltenyi Biotec Inc.	Cat No. 130-042-102
MACS Multi Stand	Miltenyi Biotec Inc.	Cat No. 130-042-303
MS Column	Miltenyi Biotec Inc.	Cat No. 130-042-201
Software and algorithms		
Fiji	Schindelin et al., 2012	https://imagej.net/Fiji
LAMA (17.07)	Malkusch and Heilemann, 2016	https://www.uni-frankfurt.de/54258347/Software
Adobe Illustrator CS6	Adobe	https://www.adobe.com/ca/products/illustrator.html
Matlab (R2022b)	Mathworks	https://www.mathworks.com/products/matlab.html
Origin 8	Origin Lab	https://www.originlab.com/index.aspx?go=PRODUCTS/Origin
Deposited Data		
MATLAB Scripts	This Paper	https://doi.org/10.20383/103.0809
Data for MATLAB Scripts	This Paper	https://doi.org/10.20383/103.0809

Supplemental Table 5. List of reagents and supplies used, software applications, and location of data repository.